

# LDA-1B: Scaling Latent Dynamics Action Model via Universal Embodied Data Ingestion

Jianguan Lyu<sup>\*1,2</sup>, Kai Liu<sup>\*2,3,4</sup>, Xuheng Zhang<sup>\*1,2</sup>, Haoran Liao<sup>2,6</sup>, Yusen Feng<sup>1,2</sup>, Wenzuan Zhu<sup>1</sup>, Tingrui Shen<sup>1</sup>, Jiayi Chen<sup>1,2</sup>, Jiazhao Zhang<sup>1,2</sup>, Yifei Dong<sup>1</sup>, Wenbo Cui<sup>2,3,4</sup>, Senmao Qi<sup>2</sup>, Shuo Wang<sup>2</sup>, Yixin Zheng<sup>2,3,4</sup>, Mi Yan<sup>1,2</sup>, Xuesong Shi<sup>2</sup>, Haoran Li<sup>3</sup>, Dongbin Zhao<sup>3</sup>, Ming-Yu Liu<sup>7</sup>, Zhizheng Zhang<sup>2,†</sup>, Li Yi<sup>5,†</sup>, Yizhou Wang<sup>1,†</sup>, He Wang<sup>1,2,†</sup>

<sup>1</sup>Peking University <sup>2</sup>Galbot <sup>3</sup>CASIA <sup>4</sup>BAAI <sup>5</sup>Tsinghua University <sup>6</sup>Sun Yat-sen University <sup>7</sup>NVIDIA

Code & Data: <https://pku-epic.github.io/LDA> \* Equal contribution † Corresponding authors

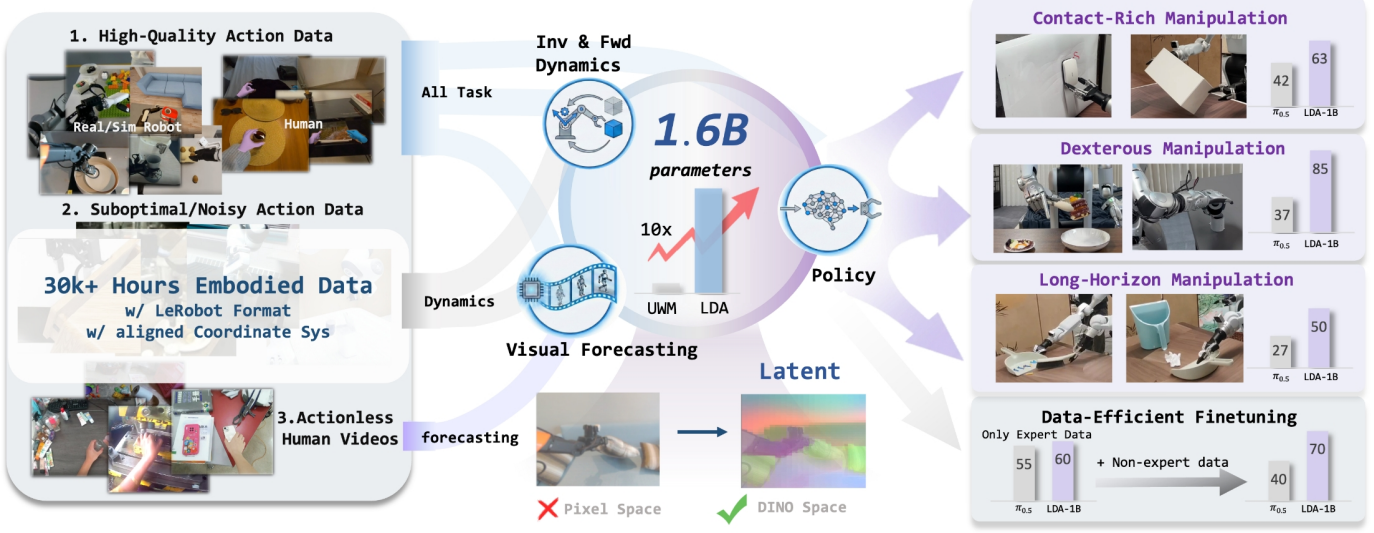


Fig. 1: We introduce LDA-1B, a 1.6 B-parameter robot foundation model scaled on over 30k hours of heterogeneous embodied data. LDA-1B unifies policy, dynamics, and visual forecasting in a structured DINO [46] latent space, allowing different data sources to play complementary roles. Beyond high-quality data alone, noisy data and actionless videos also provide valuable visual and physical priors for dynamics learning. This universal data ingestion paradigm enables stable scaling with data and model size, significantly outperforming strong baselines such as  $\pi_{0.5}$  [23] across diverse manipulation tasks.

**Abstract**—Recent robot foundation models largely rely on large-scale behavior cloning, which imitates expert actions but discards transferable dynamics knowledge embedded in heterogeneous embodied data. While the Unified World Model (UWM) formulation has the potential to leverage such diverse data, existing instantiations struggle to scale to foundation-level due to coarse data usage and fragmented datasets. We introduce LDA-1B, a robot foundation model that scales through universal embodied data ingestion by jointly learning dynamics, policy, and visual forecasting, assigning distinct roles to data of varying quality. To support this regime at scale, we assemble and standardize EI-30k, an embodied interaction dataset comprising over 30k hours of human and robot trajectories in a unified format. Scalable dynamics learning over such heterogeneous data is enabled by prediction in a structured DINO latent space, which avoids redundant pixel-space appearance modeling. Complementing this representation, LDA-1B employs a multi-modal diffusion transformer to handle asynchronous vision and action streams, enabling stable training at the 1B-parameter scale. Experiments in simulation and the real world show LDA-1B outperforms prior methods (e.g.,  $\pi_{0.5}$ ) by up to 21%, 48%, and 23% on contact-rich, dexterous, and long-horizon tasks, respectively. Notably, LDA-1B enables data-efficient fine-tuning, gaining 10% by leveraging 30% low-quality trajectories typically harmful and discarded.

## I. INTRODUCTION

Inspired by the success of Large Language Models (LLMs) and Vision-Language Models (VLMs), the robotics community has increasingly pursued general-purpose robot foundation models through large-scale pretraining [5, 41]. Most existing approaches center on scaling behavior cloning (BC), which imitates expert actions but fundamentally restricts learning to high-quality demonstrations. Consequently, a large portion of heterogeneous embodied data [42] is discarded or only weakly utilized, despite containing rich physical interaction dynamics [26].

Unified World Model (UWM) formulation [30, 60] provides an alternative by jointly optimizing dynamics, policy, and video generation within a single model, which can leverage not only expert data. Despite the potential value, existing UWM instantiations remain far from scaling to foundation-level. A major limitation lies in coarse data usage: heterogeneous embodied data are often treated uniformly, without differentiating their roles by quality or supervision, which underutilizes transferable dynamics knowledge. In addition, the community lacks ready-to-use large-scale datasets that

unify varying-quality data with consistent formats and aligned action representations. Furthermore, UWM represent future state in pixel space, entangling dynamics learning with redundant appearance modeling. Subtle variations in illumination, texture, background clutter, or camera viewpoint can dominate the training objective, making large-scale training inefficient and hindering the learning of interaction-relevant dynamics.

To overcome these limitations, we introduce **LDA-1B**, a robot foundation model that scales via *universal embodied data ingestion*. In this framework, heterogeneous data play distinct yet complementary roles: actionless human videos supervise visual forecasting [38, 37, 25], lower-quality trajectories primarily inform dynamics learning, and high-quality trajectories support both policy and dynamics. To realize this approach at scale, we assemble **EI-30k**, a large-scale embodied interaction dataset with over 30k hours of human and robot trajectories across real and simulated environments, standardized in format and aligned in action representation. Scalable learning on such diverse data is facilitated by a structured **DINO latent space** [46, 59, 22], which reduces redundant appearance modeling [38, 25], and a multi-modal diffusion transformer that aligns asynchronous visual and action prediction. By combining this ingestion strategy, dataset, latent representation, and model architecture, LDA-1B achieves stable training at the 1B-parameter scale while maximizing data utilization.

We evaluate LDA-1B on challenging RoboCasa-GR1 benchmark and a diverse set of real-world tasks involving both grippers and high-DoF dexterous hands [56]. LDA-1B consistently outperforms  $\pi_{0.5}$ , achieving **21%** gains on contact-rich manipulation, benefiting from improved dynamics understanding and **48%** gains on dexterous manipulation, benefiting from effective utilization of human data. Moreover, under a mixed-quality fine-tuning setting, LDA-1B improves data efficiency by **10%** through leveraging low-quality trajectories that are detrimental to baseline methods. These results highlight universal embodied data ingestion and unified latent dynamics learning as a scalable alternative to behavior-cloning-centric robot pretraining. In summary, our contributions are threefold:

- We propose LDA-1B, a scalable robot foundation model that learns generalizable interaction dynamics through unified latent dynamics pretraining.
- We construct EI-30k, a large-scale embodied interaction dataset covering diverse embodiments, environments, data qualities, with aligned end effector coordinate system.
- We demonstrate that LDA-1B achieves superior generalization and robustness across a wide range of settings, including simulation and real-world environments, contact-rich manipulation, dexterous manipulation, and long-horizon manipulation.

## II. RELATED WORK

**Robot Foundation Models.** Recent robot foundation models predominantly adopt the Behavior Cloning paradigm. As summarized in Table I, representative approaches including

Model	Data Src.	#Data	Action	Quality	Train.	Param.
$\pi_{0.5}$ [23]	Tele.	10k+	High		BC	3B
RDT [32]	Tele.	<10k	High		BC	1B
GraspVLA [14]	Sim.	20k+	High		BC	2B
InternVLA-M1 [11]	Sim.	<10k	High		BC	3B
Being-H0 [35]	Hum.	<10k	Mixed		Aln. + BC	14B
InternVLA-A1 [9]	Het.	10k+	High		VF + BC	3B
GR00T-N1.6 [40]	Het.	<10k	Mixed		LA + BC	1B
UniVLA [7]	Het.	<10k	Mixed		LA + BC	7B
<b>LDA-1B</b>	Het.	<b>30k+</b>	Mixed		UWM[60]	1B

TABLE I: **Comparison of Representative Robot Foundation Models.** This table compares the proposed LDA with recent robot foundation models in terms of data source, data quantity, action quality, training paradigm, and the number of trainable model parameters (excluding frozen components). Data source abbreviations are as follows: Tele.=teleoperation, Sim.=simulation, Hum.=human demonstration, and Het.=heterogeneous data. Training paradigm abbreviations include: BC=behavior cloning, VF=visual foresight, Aln.=alignment, LA=latent action modeling, and UWM=unified world model. Only embodied interaction data are considered, excluding internet-scale VQA data.

$\pi_0$  [4], RDT [32], and InternVLA [11]rely heavily on high-quality teleoperation or simulation data, which fundamentally constrains their scalability. Hybrid methods such as Being-H0 [35] and UniVLA [7] attempt to incorporate heterogeneous data with mixed quality; however, they largely depend on action alignment or auxiliary pretrained latent action models, limiting the effective data scale to around 6k hour embodied data. In contrast, LDA-1B breaks this ceiling by adopting a unified world model formulation, enabling efficient ingestion of up to 30k hours of mixed-quality embodied data.

**Unified Video Action Models.** Recent works have explored joint modeling dynamics and policy for embodied decision making. Methods such as DyWA [36], FLARE [58], and the WorldVLA series [10, 24] demonstrate that co-training next-state prediction and policy learning can improve generalization in interactive environments. To enrich dynamics modeling, UWM [60] and UVA [30] further propose optimizing multiple objectives jointly, including video generation, forward and inverse dynamics, and action prediction. Concurrent with our work, Motus [3] adopt UWM paradigm and integrate priors from pretrained VLM and video generation models. Despite their promising results, these approaches typically operate directly in pixel space and do not explicitly consider the roles of data quality, scale, or heterogeneity during training, which limits their ability to fully exploit large-scale, mixed-quality interaction data for robust dynamics learning.

**Large-Scale Embodied Interaction Datasets.** The progress in embodied ai relies on large-scale embodied datasets. Many widely used datasets are collected via teleoperation on real robots [4, 23, 27, 31] or generated in simulation [14, 11], providing high-quality action-labeled trajectories. Beyond robot-collected data, recent works explore human-centric embod-

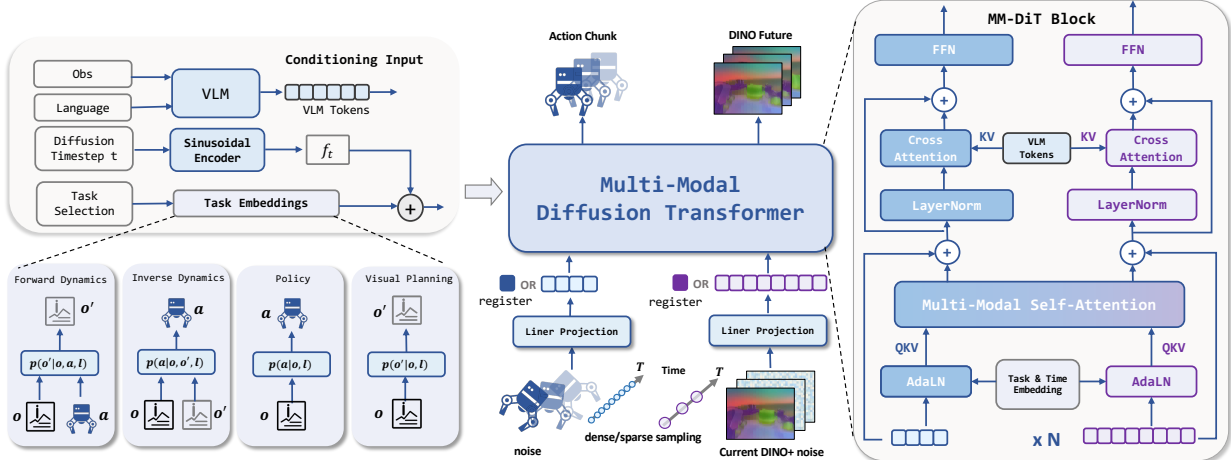


Fig. 2: **Architecture of LDA.** LDA jointly denoises action chunks and future visual latent under multiple co-training objectives, including policy learning, forward dynamics, inverse dynamics, and visual forecasting. Conditioned on VLM tokens, diffusion timesteps, and task embeddings, the model adopts a multimodal diffusion transformer architecture, where action and visual experts are decoupled and interact through a shared self-attention layer.

ied datasets, such as egocentric recordings with hand actions [53, 35]. While these datasets significantly expand data diversity, many are either not publicly released or provide limited action supervision, making them difficult to directly integrate with robot learning pipelines. More broadly, existing embodied datasets are highly fragmented: some are closed-source, others are open but vary substantially in data formats, sensor configurations, action representations, and annotation quality. This lack of standardization poses a major obstacle to large-scale data aggregation and unified training. In contrast, our work introduces EI-30k, a large-scale embodied interaction dataset that unifies diverse data sources including robot and human trajectories from both real-world and simulated environments under consistent data formats and aligned action representations.

### III. LATENT DYNAMICS ACTION MODEL

#### A. Preliminary: Unified World Models

Given the current observation  $o_t$  (typically an RGB image), UWM [60] jointly models multiple conditional distributions over future observations  $o_{t+1:t+k}$  and action chunk  $a_{t+1:t+k}$ , enabling unified learning of:

- 1) Policy:  $p(a_{t+1:t+k} | o_t)$
- 2) Forward Dynamics:  $p(o_{t+1:t+k} | o_t, a_{t+1:t+k})$
- 3) Inverse Dynamics:  $p(a_{t+1:t+k} | o_{t:t+k})$
- 4) Visual Planning:  $p(o_{t+1:t+k} | o_t)$

Concretely, UWM [60] instantiates this framework using a joint diffusion model that predicts noise for both actions and future observations:

$$(\epsilon_a^\theta, \epsilon_o^\theta) = s_\theta(o, a_{t_a}, o'_{t_o}, t_a, t_{o'}) ,$$

where  $t_a$  and  $t_o$  are independently sampled diffusion timesteps for actions and observations, and  $\tilde{a}_{t_a}$ ,  $\tilde{o}_{t_o}$  denote their corresponding noisy inputs. The model is trained with a standard DDPM [20] objective, jointly denoising future actions and

observations conditioned on  $o_t$ . We further extend this formulation by introducing language  $\ell$  conditioning through a VLM, enabling instruction-guided action and observation prediction.

#### B. Universal Data Ingestion via Multi-task Co-training

We adopt a *universal data ingestion* regime to jointly train the unified objectives described above, allowing heterogeneous embodied data to contribute according to their supervision quality. Specifically, high-quality robot and human demonstrations are co-trained with all objectives, supporting both action policy learning and dynamics modeling. Lower-quality trajectories, which may contain suboptimal or noisy actions, are used exclusively for dynamics and visual forecasting, where accurate action optimality is not required. In addition, we leverage large-scale human manipulation videos without action annotations to train the visual forecasting objective, providing supervision for instruction-conditioned future state prediction. This role-aware data usage prevents overfitting to expert-only behaviors and enables scalable learning of transferable dynamics and action representations.

To implement differentiated objectives within a single diffusion model, we introduce four learnable *task embeddings* and two learnable *register tokens*. Each task embedding corresponds to a specific training objective (policy, forward dynamics, inverse dynamics, or visual forecasting) and is added to the diffusion timestep embedding  $f_t$  to condition the denoising process. The learnable register tokens one for action and one for visual states serve as placeholders for modalities that are absent in a given task. For example, during policy training, the model receives noisy action tokens along with a visual register token representing the unobserved future state; in contrast, visual forecasting uses noisy future visual tokens with an action register token. This design enables a unified architecture to flexibly support different input/output structures without modifying the network topology. Overall,

the model predicts a denoising vector field  $v_a^\theta$  under different task conditions and is trained using a flow-matching objective:

$$\begin{aligned} l_{\text{action}}^\theta &= \mathbb{E}_{(\mathbf{o}_{t:t+k}, \mathbf{a}_{t+1:t+k}, \ell) \sim \mathcal{D}} \|v_a^\theta - (\epsilon_a - \mathbf{a}_{t+1:t+k})\|_2^2, \\ &\quad \tau_a \sim \mathcal{U}(0, T_\tau) \\ &\quad \epsilon_a \sim \mathcal{N}(\mathbf{0}, \mathbf{I}) \\ l_{\text{obs}}^\theta &= \mathbb{E}_{(\mathbf{o}_{t:t+k}, \mathbf{a}_{t+1:t+k}, \ell) \sim \mathcal{D}} \|v_o^\theta - (\epsilon_o - \mathbf{o}_{t+1:t+k})\|_2^2, \\ &\quad \tau_o \sim \mathcal{U}(0, T_\tau) \\ &\quad \epsilon_o \sim \mathcal{N}(\mathbf{0}, \mathbf{I}) \\ l^\theta &= l_{\text{action}}^\theta + l_{\text{obs}}^\theta. \end{aligned} \quad (1)$$

During training, action and visual losses are selectively activated according to the task specification, allowing heterogeneous data to contribute under appropriate supervision. At inference time, the same model can be flexibly invoked for different objectives by specifying the task embedding and corresponding inputs.

### C. Representation of Predictive Targets

We represent predictive targets future visual states and actions in a unified format to maximize knowledge sharing across heterogeneous datasets. For visual prediction, we adopt latent features extracted from a pretrained DINO [46] encoder, rather than VAE-based pixel-space representations. DINO latents encode high-level semantic and spatial structure while suppressing background noise and low-level visual variations, which facilitates learning scene dynamics that generalize across diverse environments and object configurations.

For actions, we define a unified hand-centric action space based on end-effector motion, consisting of delta wrist poses and finger configurations. For parallel-jaw grippers, the finger state is represented by a single degree-of-freedom gripper width, while for multi-finger dexterous hands, finger configurations are described using keypoints expressed in the wrist coordinate frame. This design enables consistent action modeling across different embodiments and manipulation platforms.

To model temporal dynamics, visual states and actions are organized as two synchronized temporal streams with different sampling rates. Visual observations are sampled at 3hz, a lower frequency than actions, 10 hz. This reduces redundant computation from highly correlated consecutive frames while preserving fine-grained action dynamics, allowing the model to maintain coherent temporal alignment between fast-varying control signals and slower-evolving visual states.

### D. Architecture: MM-DiT

We adopt a Multi-Modal Diffusion Transformer (MM-DiT) to jointly denoise action chunks and predict future visual features within a unified diffusion framework (Fig. 2). The model operates on heterogeneous tokens while sharing a common Transformer backbone. Conditioning inputs include the current observation, language instruction, diffusion timestep, and task specification. Observations and language are encoded by a pretrained VLM into conditioning tokens. The diffusion timestep is encoded using a sinusoidal embedding, and task information is represented by a learned task embedding. All

conditioning signals are injected into each Transformer block via adaptive layer normalization (AdaLN [43]).

Actions are organized as fixed-length chunks and corrupted with Gaussian noise. Future visual features (DINO [46] features) are noised in parallel. Both modalities are projected into token embeddings through modality-specific linear layers and processed jointly by MM-DiT. Each MM-DiT block applies multi-modal self-attention over concatenated action and visual tokens, enabling cross-modal interaction. Modality-specific QKV projections and FFNs are retained to preserve inductive biases, while attention is shared across modalities. Language tokens are incorporated via cross-attention to provide high-level semantic guidance. Finally, modality-specific output heads predict denoised action sequences and future visual features.

### E. Pre-training and Post-training

**Pre-training Configurations.** Our model is trained on a server cluster equipped with 48 NVIDIA H800 GPUs. The training process contains 400k iterations, resulting in a total computational cost of 4,608 GPU hours. To preserve the generalization capability and visual representation quality of the pre-trained foundation models, we keep the parameters of the VLM [52] and the DINO [46] encoder frozen throughout the pre-training process, updating the MM-DiT and action encoder/decoder. This design ensures that the model can learn from new data without degrading the core abilities of the base models in cross-modal understanding and fine-grained visual feature extraction.

**Data-Efficient Finetuning.** To adapt the model to target embodiments and tasks for real-world deployment, we introduce a lightweight post-training stage. This stage follows the same data regime as pretraining and effectively leverages naturally collected teleoperation data of mixed quality, without requiring expert-level demonstrations. Compared to prior finetuning pipelines that rely on carefully curated expert datasets, our method directly utilizes unfiltered teleoperation data, substantially improving data efficiency and reducing the cost of data collection and annotation, thereby facilitating practical deployment.

## IV. EMBODIED INTERACTION DATASET (EI-30K)

We introduce the Embodied Interaction Dataset (EI-30K), a large-scale collection of embodied interaction trajectories totaling over 30k hours. It consists of 8.03k hours of real-world robot data, 8.6k hours of simulated robot data, 7.2k hours of human demonstrations with actions, and 10k hours of actionless human videos. All subdatasets are annotated with explicit quality labels, enabling systematic analysis across different fidelity levels and supporting quality-aware learning.

**Data Unification.** EI-30K consolidates datasets from heterogeneous platforms and tasks, which vary in storage formats, sensor modalities, and annotations. All data are converted into the LeRobot format, providing a unified representation of observations, actions, and language. This standardization facilitates plug-and-play training, flexible data composition, and

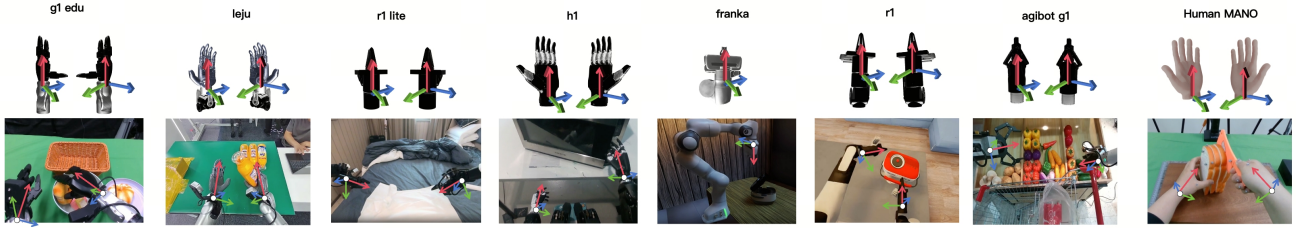


Fig. 3: **Aligned End Effector Coordinate Systems.** We manually align coordinate frames across diverse robot and human embodiments to ensure consistency. This shared representation enables joint learning from heterogeneous interaction data.

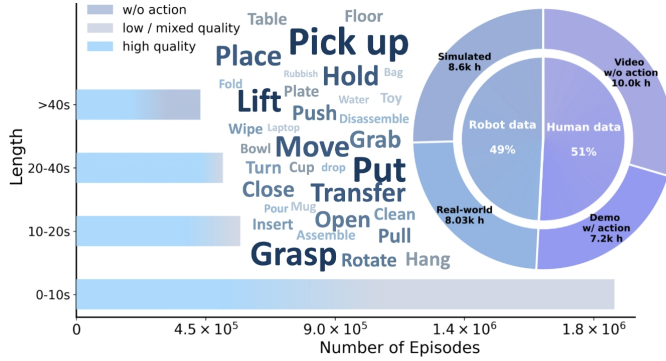


Fig. 4: **Statistics of EI-30K.** The dataset contains more than 30k hours of diverse human and robot interaction data (right). It spans varying episode lengths (left) and a rich set of manipulation tasks (center).

seamless integration of additional annotations, while greatly reducing engineering overhead for handling diverse sources.

**Aligned Action Representation.** To support consistent modeling of physical interactions across embodiments, all available action annotations are expressed as hand-centric motion in a shared coordinate frame (Fig. 3). For robots, this includes the 6-DoF end-effector pose plus gripper width or dexterous hand joints. For humans, the 6-DoF wrist pose and full MANO [45] hand parameters are recorded. Camera extrinsics are retained to decouple hand motion from egocentric head motion. All coordinate frames are manually aligned to ensure geometric consistency across datasets, enabling joint learning from both human and robot trajectories.

**Quality Annotation and Cleaning.** EI-30K applies systematic cleaning and quality-aware annotation. Language annotations are normalized using a vision-language model to ensure semantic consistency. Motion segments without meaningful hand-object interaction are removed, e.g., head-only or idle segments in egocentric videos. Each trajectory is assigned a quality label based on action accuracy, and annotation completeness. Unlike aggressive filtering, low-quality trajectories are preserved, allowing downstream models to exploit the full spectrum of data through quality-aware training.

## V. EXPERIMENTS

### A. Simulation Experiments

**Benchmark and Baselines.** We evaluate our method on RoboCasa-GR1 [39], a simulated kitchen benchmark featuring

Model	Vis. Rep.	MMDiT	VLM	Success Rate ↑
GR00T-N1.6[40]	-	-	Cosmos	47.6
StarVLA[47]	-	-	Qwen3vl[52]	47.8
GR00T-EI30k	-	-	Qwen3vl	51.3
UWM-0.1B[60]	VAE	✗	-	14.2
UWM-1B	VAE	✗	Qwen3vl	19.3
UWM(MM-DiT)	VAE	✓	Qwen3vl	20.0
LDA(DiT)	DINO	✗	Qwen3vl	48.9
LDA-0.5B	DINO	✓	Qwen3vl	50.7
LDA-1B	DINO	✓	Qwen3vl	<b>55.4</b>

TABLE II: Results on RoboCasa-GR1 [39] and impact of state representation (VAE vs. DINO [46]) model size the MM-DiT architecture on task success rates.

24 tabletop rearrangement and articulated-object manipulation tasks with the GR-1 humanoid robot and Fourier dexterous hands. The benchmark provides challenging and realistic settings that require high-DoF dexterous manipulation from egocentric RGB observations captured by a head-mounted camera. Following the GR00T [40] evaluation protocol, we finetune all models using 1,000 trajectories per task and evaluate each task with 51 trials, reporting average success rates. We compare LDA against GR00T and its strong variants, as well as UWM [60], under matched training paradigms and data. To ensure a fair comparison in terms of model capacity and pretraining, we reproduce a strong GR00T baseline (denoted as GR00T-EI10k) with 1B parameters, pretrained on our curated EI-30k high-quality subset and using Qwen3-VL as the VLM encoder.

**Comparison with Baselines.** As shown in Table II, the original GR00T-N1.6 [40] with 3B parameters achieves a success rate of 47.6%. When pretrained on our curated EI-30k dataset, the reproduced GR00T-EI10k with 1B parameters shows a clear improvement, reaching 51.3%, highlighting the impact of high-quality embodied data. Under the same parameter budget, LDA further improves the success rate to 55.4%. These results indicate that, beyond data quality and parameter scaling, jointly learning actions and dynamics within a unified model provides additional gains when pretrained on mixed-quality data.

**Ablation Study.** We further analyze key design choices under identical training data and optimization settings. UWM [60], despite jointly predicting actions and dynamics, achieves only 14.2% success due to limited model capacity and the use



Fig. 5: Real-World Manipulation Demonstrations Across Multiple Robotic Platforms and End-Effectors. Galbot G1 equipped with a Sharpa dexterous hand (top-left), Unitree G1 with a BrainCo dexterous hand (middle and bottom-left), and Galbot G1 with a two-finger gripper (right).

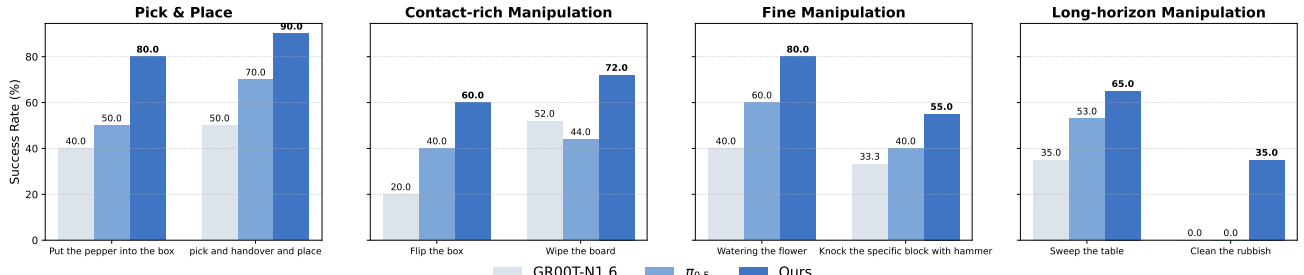


Fig. 6: Success Rate Comparison on Real-World Gripper Manipulation Tasks. All models are few-shot fine-tuned on Galbot and evaluated on eight tasks spanning Pick & Place, Contact-rich, Fine, and Long-horizon manipulation. LDA consistently outperforms GR00T-N1.6 [40] and  $\pi_{0.5}$  [23].

of entangled VAE latent representations. Scaling UWM to 1B parameters or replacing its DiT backbone with our MM-DiT yields only marginal improvements (19.3% and 20.0%, respectively), suggesting that architectural constraints fundamentally limit its performance. In contrast, replacing pixel-space VAE latents with DINO [46] representations leads to a substantial performance gain (20.0%  $\rightarrow$  55.4%), highlighting the importance of semantically structured latent spaces for effective scaling. Finally, removing the proposed MM-DiT architecture or reducing the model size to 0.5B parameters results in performance drops of 6.5% and 4.7%, respectively, confirming the effectiveness of the multi-expert design and its favorable scaling behavior.

## B. Real-world Experiments

To validate the scalability and robustness of LDA-1B, we conduct extensive real-world experiments focusing on few-shot adaptation to new embodiments, dexterous manipulation, and data efficiency under mixed-quality supervision.

**Real-World Robot and Task Setup.** We evaluate our method on two humanoid platforms: Galbot G1 and Unitree G1. Galbot G1 is equipped with either a two-finger gripper or

22-DoF Sharpa dexterous hands, while Unitree G1 uses 10-DoF BrainCo hands. Across all configurations, the policy receives only egocentric RGB observations from a head-mounted camera. We evaluate four categories of manipulation tasks under the gripper setting, *Pick and Place*, *Contact-rich Manipulation*, *Fine Manipulation*, and *Long-horizon Manipulation* covering diverse contact dynamics and temporal horizons. Representative tasks include *Beat Block*, *Flip Box*, *Handover*, *Pick-and-Place (Pepper)*, *Sweep Table*, *Clean Rubbish*, *Water Flower*, and *Wipe Board*. Dexterous manipulation further includes tool-use tasks such as pulling a nail with a hammer and flipping bread with a spatula, which require precise force control and coordinated finger motion. Qualitative demonstrations are shown in Fig. 5. For each task, we collect 100 teleoperated trajectories without enforcing expert-level execution. As a result, the dataset naturally exhibits mixed quality: approximately 50–80% of trajectories correspond to expert behavior, while the remainder contain suboptimal actions such as pauses, retries, or inefficient motion patterns.

**Baselines and Finetuning Protocol.** We compare LDA-1B against two strong baselines,  $\pi_{0.5}$  [23] and GR00T [40]. To ensure stable and competitive performance, baseline models

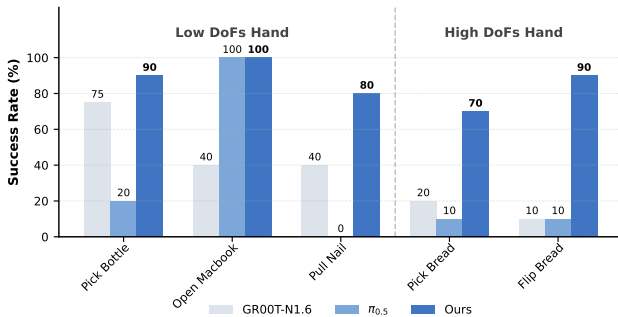


Fig. 7: **Success Rate Comparison on Real-World Dexterous Manipulation Tasks** We evaluate the real-world performance of our model against baselines (GR00T-N1.6 and  $\pi_{0.5}$ ) on 3 low DoFs hand (BrainCo) tasks and 2 high DoFs hand (Sharpa) tasks. Ours (dark blue) consistently outperforms baselines especially on fine dexterous task (pull nails) and high DoFs tasks.

Method	Pick & Place		
	Object	Background	OOD Pos.
$\pi_{0.5}$	26.7	20.0	6.7
GR00T	40.0	40.0	20.0
Ours	<b>60.0</b>	<b>60.0</b>	<b>40.0</b>

TABLE III: **Robust Generalization under visual and spatial perturbations.** LDA-1B maintains 60.0% success across unseen objects, backgrounds, and OOD positions, demonstrating effective focus on task-critical affordances over visual noise through latent dynamics pretraining.

are finetuned exclusively on the filtered expert subset. In contrast, LDA-1B leverages all collected trajectories and learns directly from the full mixed-quality distribution via our Universal Embodied Data Ingestion mechanism.

**Results on Gripper Manipulation.** We first evaluate few-shot adaptation by deploying LDA-1B on the Galbot G1, which is excluded from our EI-30k pretraining dataset. As shown in Fig. 6, LDA-1B consistently outperforms all baselines across task categories. On simple pick-and-place tasks, LDA-1B achieves success rates of 80%–90%, indicating effective few-shot adaptation to a new robot embodiment. The performance gap widens substantially in contact-rich and long-horizon scenarios. For instance, the *Clean the Rubbish* task requires coordinated dual-arm manipulation, tool usage (dustpan), and sequential object transfer into a trash bin, where errors can easily accumulate over time. In this setting, LDA-1B achieves a 35% success rate, while both GR00T and  $\pi_{0.5}$  fail entirely (0%). This result suggests that latent dynamics modeling enables LDA to better anticipate action-induced state transitions, maintain temporal consistency, and recover from intermediate failures in extended manipulation sequences.

**Results on Dexterous Manipulation.** We further evaluate LDA-1B on both low-DoF and high-DoF dexterous manipulation tasks, as reported in Fig. 7. On low-DoF tasks such as *Pull Nail*, which requires precise motion direction and

Method	Place the pen into the box		Bimanually remove the lid	
	63 High	63 High + 37 Low	66 High	66 High + 34 Low
$\pi_{0.5}$	60	40 (20↓)	50	40 (10↓)
Ours	<b>70</b>	<b>80 (10↑)</b>	<b>50</b>	<b>60 (10↑)</b>

TABLE IV: **Data-efficient mixed-quality finetuning.** LDA-1B improves success rates by +10% on both tasks when incorporating low-quality trajectories, while  $\pi_{0.5}$  degrades significantly, demonstrating effective utilization of noisy data for enhanced generalization.

stable contact maintenance between the hammer and the nail, LDA-1B achieves 80% success, reliably localizing targets and adjusting sensitive actions, whereas  $\pi_{0.5}$  largely fails. On high-DoF tasks such as *Flip Bread*, which involve high-dimensional control, continuous contact, and coordinated wrist motion, LDA-1B attains 90% success, while  $\pi_{0.5}$  reaches only 10%. These results demonstrate that pretraining on large-scale human data provides strong latent priors for dexterous control, enabling precise finger coordination and object reorientation with limited robot data. In contrast, baseline policies struggle to generalize as action dimensionality and contact complexity increase.

**Generalization Ability.** To evaluate the generalization of our policy, we test pick and place task under three conditions: novel objects, unseen backgrounds, and out-of-distribution (OOD) starting position, shown as Fig 8. As summarized in Table III, our model maintains high success rates despite visual and spatial perturbations. The large-scale latent dynamics pretraining allows the model to ignore visual distractors (background changes) while focusing on relevant object affordances, demonstrating strong generalization relative to baselines.

**Data-Efficient Finetuning.** We analyze the value of mixed-quality data ingestion during finetuning stage, by post-training on two splits: (1) High-Quality Only (expert data), and (2) High + Low Quality (all 100 trajectories). As shown in Table IV, while baseline models degrade when low-quality data is added, LDA-1B effectively leverages these noisy trajectories, boosting performance with 10%, substantially improving data efficiency and reducing the cost of data collection and annotation for practical deployment.

### C. Analysis of Scaling Effects

To analyze the scaling behavior of LDA, we systematically vary model capacity, data composition, and training objectives. All models are evaluated on an unseen test set sampled from a held-out subset of *Agibot World* [6]. We report the action prediction L1 error as the primary metric, which serves as a stable and reproducible proxy for real-world performance. Fig. 10 summarizes the results under four training configurations: (i) *Policy Only*, (ii) *Policy + Visual Forecasting*, (iii) *Policy with Forward and Inverse Dynamics*, and (iv) the full co-training framework (*Ours*). These experiments jointly reveal how LDA scales under heterogeneous supervision and increasing model capacity.



Fig. 8: Generalization evaluation setup on Pick and Place task

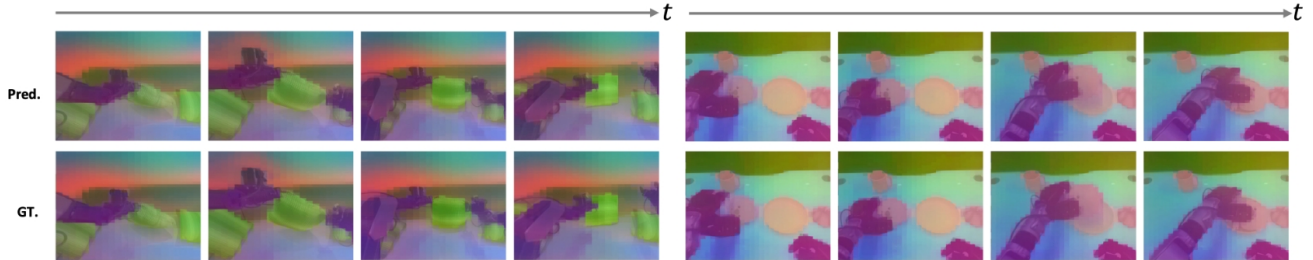


Fig. 9: **Visualization of latent forward dynamics.** Our model generates accurate future visual representations (top) aligned with ground truth (bottom) across time steps, capturing semantic object structure and motion dynamics

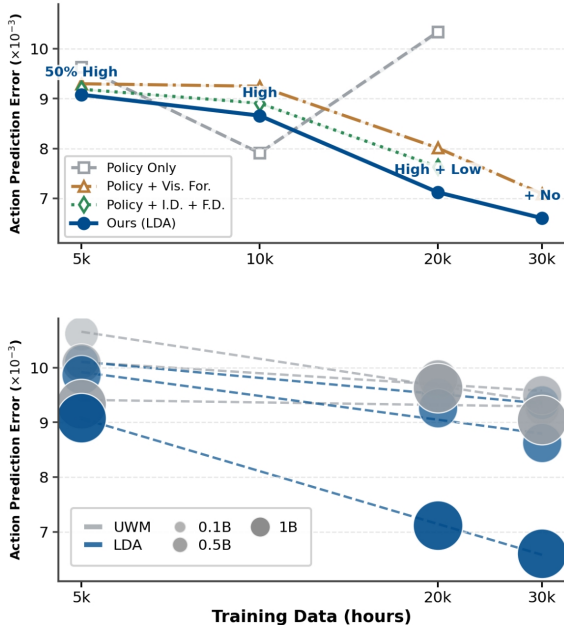


Fig. 10: Scaling Analysis of LDA, evaluated by action prediction error on unseen test set. Top: Action prediction error decreases to 6.6 with 30k hours of training data, demonstrating effective utilization of diverse data sources. Bottom: LDA consistently outperforms UWM across model sizes (0.1B → 1B) with increasing training data, while the baseline saturates rapidly.

**Effectiveness of Universal Data Ingestion.** Effectively leveraging heterogeneous embodied data requires jointly scaling both data sources and training objectives. As shown in Fig. 10, LDA achieves its best performance only when all supervision signals—policy learning, dynamics modeling, and visual forecasting—are optimized together. When either the data scale or the training objectives are reduced, performance degrades noticeably. Using only action-labeled trajectories with a *Policy Only* objective (grey line), increasing the dataset size yields

unstable behavior: while moderate scaling initially reduces error, incorporating lower-quality data leads to performance degradation. Similarly, partial co-training variants that exclude either dynamics or visual forecasting objectives (green and brown lines) improve robustness but fail to fully exploit the available data. In contrast, the full co-training framework (blue line) exhibits consistent improvement as additional heterogeneous data is introduced. Notably, even after all action-labeled trajectories are exhausted, adding 10k actionless videos continues to reduce prediction error. This indicates that LDA can extract useful supervisory signals from low-quality data and non-action data through latent dynamics and visual forecasting, rather than treating such data as noise. Overall, these results demonstrate that Universal Data Ingestion is most effective when heterogeneous data and co-training objectives are scaled together, enabling LDA to fully utilize mixed-quality supervision.

**Effectiveness of Latent Representation.** Although both LDA and UWM incorporate dynamics-related supervision, their scaling behaviors diverge substantially due to differences in the structure of their latent spaces. As shown in Fig. 10, UWM quickly saturates as data scale and model capacity increase, with additional supervision yielding diminishing or even negative returns. This indicates that simply increasing data or parameters is insufficient when the latent space cannot support compositional and causal reasoning. This limitation stems from UWM’s VAE-derived latent representation, which entangles appearance, geometry, and dynamics at a low-level feature granularity. Such entanglement restricts the model’s ability to factorize action-induced state transitions and prevents effective reuse of heterogeneous supervision during scaling. In contrast, LDA operates in a semantically structured latent space obtained from large-scale visual pretraining. This representation preserves object-level semantics and spatial coherence, enabling dynamics learning to scale smoothly with increased model capacity, richer training objectives, and more diverse datasets.

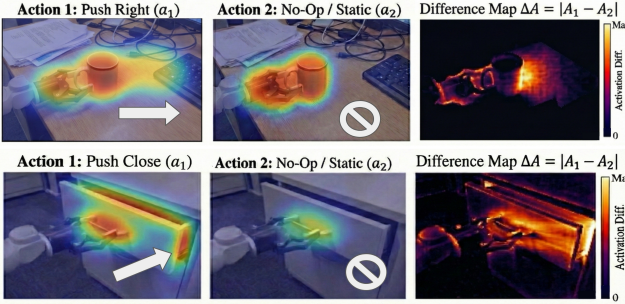


Fig. 11: Attention Heat Map: "Push Right"(top) highlights the mug's leading edge and trajectory; "Push Close"(bottom) concentrates on the contact surface. The model attends exclusively to movable regions while ignoring irrelevant background clutter.

**Effectiveness of Model Scaling.** Beyond data scale, LDA exhibits consistent and predictable improvements as model capacity increases. As shown in Fig. 10, scaling the model from 0.1B to 0.5B and further to 1B parameters leads to monotonic reductions in action prediction error under the full co-training framework. This indicates that LDA can effectively absorb additional capacity to model increasingly complex actiondynamics relationships when sufficient heterogeneous supervision is available. The results highlight a promising scaling paradigm in which model capacity, training objectives, and heterogeneous embodied data are jointly aligned, enabling reliable performance gains.

#### D. Analysis of Dynamics Learning

**Qualitative Analysis of Latent Forward Dynamics.** Beyond quantitative prediction errors, we qualitatively examine the forward dynamics learned by LDA, visualized via PCA projections of DINO feature embeddings. As shown in Fig. 16, the model produces coherent future-state predictions that respect physical constraints such as object permanence, contact continuity, and motion consistency under the applied action. Notably, the predicted dynamics focus on task-relevant objects while remaining invariant to visual distractors that do not influence the control loop. This suggests that LDA learns a dynamics-aware latent world model, capturing how actions causally propagate through the scene rather than merely extrapolating visual appearance.

**Action-Conditioned Attention.** To interpret how LDA reasons about action-induced state transitions, we visualize attention maps conditioned on different action primitives. As shown in Fig. 11, we compare the attention patterns induced by an active motion command ( $a_1$ ) with those under a static *No-Op* command ( $a_2$ ), and compute their difference to reveal action-specific visual grounding. Across tasks, LDA consistently attends to regions that are causally relevant to the commanded interaction. In the *Push Right* scenario, the attention difference highlights the leading edge of the mug and the anticipated motion direction, reflecting awareness of object displacement. In the *Push Close* task, attention concentrates on the drawer

surface where contact and force application are expected. Importantly, background clutter and visually salient but non-interactive regions are largely suppressed. These results indicate that LDA conditions visual attention on the physical consequences of actions, selectively focusing on regions that drive state transitions rather than static appearance.

## VI. CONCLUSION, LIMITATION AND FUTURE DIRECTION

We present **LDA-1B**, a robot foundation model that scales latent dynamics learning via universal embodied data ingestion. By assigning heterogeneous data distinct roles and leveraging over **30k hours** of human and robot trajectories in the EI-30k dataset, LDA-1B learns dynamics in a structured DINO latent space and employs a mixed-frequency multimodal diffusion transformer, enabling stable training at the **1B-parameter** scale. Experiments show strong performance across diverse manipulation and long-horizon tasks, as well as data-efficient fine-tuning on imperfect trajectories. Limitations include the reliance on fixed DINO visual features and predominantly egocentric camera viewpoints, which may constrain generalization to new visual perspectives and multi-modal signals. Future work includes jointly learning visual representations and latent dynamics, extending to richer sensory modalities, automatically optimizing data roles, and fostering broader community adoption of scalable, heterogeneous data-driven robot foundation models.

## ACKNOWLEDGMENTS

We thank Caowei Meng for collecting teleoperation data; Haoran Liu and Jiayi Su for their assistance in early-stage exploration; Yu-Wei Chao and Shengliang Deng for fruitful discussions; and Junkai Zhao for providing experimental equipment.

## REFERENCES

- [1] Build AI. Egocentric-10k, 2025. URL <https://huggingface.co/datasets/builddotai/Egocentric-10K>.
- [2] Prithviraj Banerjee, Sindi Shkodrani, Pierre Moulon, Shreyas Hampali, Shangchen Han, Fan Zhang, Linguang Zhang, Jade Fountain, Edward Miller, Selen Basol, et al. Hot3d: Hand and object tracking in 3d from egocentric multi-view videos. In *Proceedings of the Computer Vision and Pattern Recognition Conference*, pages 7061–7071, 2025.
- [3] Hongzhe Bi, Hengkai Tan, Shenghao Xie, Zeyuan Wang, Shuhe Huang, Haitian Liu, Ruowen Zhao, Yao Feng, Chendong Xiang, Yinze Rong, et al. Motus: A unified latent action world model. *arXiv preprint arXiv:2512.13030*, 2025.
- [4] Kevin Black, Noah Brown, Danny Driess, Adnan Esmail, Michael Equi, Chelsea Finn, Niccolò Fusai, Lachy Groom, Karol Hausman, Brian Ichter, et al.  $\pi_0$ : A vision-language-action flow model for general robot control. *arXiv preprint arXiv:2410.24164*, 2024.
- [5] Anthony Brohan, Noah Brown, Justice Carbajal, Yevgen Chebotar, Joseph Dabis, Chelsea Finn, Keerthana

Gopalakrishnan, Karol Hausman, Alex Herzog, Jasmine Hsu, et al. Rt-1: Robotics transformer for real-world control at scale. *arXiv preprint arXiv:2212.06817*, 2022.

[6] Qingwen Bu, Jisong Cai, Li Chen, Xiuqi Cui, Yan Ding, Siyuan Feng, Xindong He, Xu Huang, et al. Agibot world colosseo: A large-scale manipulation platform for scalable and intelligent embodied systems. In *2025 IEEE/RSJ International Conference on Intelligent Robots and Systems (IROS)*. IEEE, 2025.

[7] Qingwen Bu, Yanting Yang, Jisong Cai, Shenyuan Gao, Guanghui Ren, Maoqing Yao, Ping Luo, and Hongyang Li. Univla: Learning to act anywhere with task-centric latent actions. *arXiv preprint arXiv:2505.06111*, 2025.

[8] Remi Cadene, Simon Alibert, Alexander Soare, Quentin Gallouedec, Adil Zouitine, Steven Palma, Pepijn Kooijmans, Michel Aractingi, Mustafa Shukor, Dana Aubakirova, Martino Russi, Francesco Capuano, Caroline Pascal, Jade Choghari, Jess Moss, and Thomas Wolf. Lerobot: State-of-the-art machine learning for real-world robotics in pytorch. <https://github.com/huggingface/lerobot>, 2024.

[9] Junhao Cai, Zetao Cai, Jiafei Cao, Yilun Chen, Zeyu He, Lei Jiang, Hang Li, Hengjie Li, Yang Li, Yufei Liu, et al. Internvla-a1: Unifying understanding, generation and action for robotic manipulation. *arXiv preprint arXiv:2601.02456*, 2026.

[10] Jun Cen, Chaohui Yu, Hangjie Yuan, Yuming Jiang, Siteng Huang, Jiayan Guo, Xin Li, Yibing Song, Hao Luo, Fan Wang, et al. Worldvla: Towards autoregressive action world model. *arXiv preprint arXiv:2506.21539*, 2025.

[11] Xinyi Chen, Yilun Chen, Yanwei Fu, Ning Gao, Jiaya Jia, Weiyang Jin, Hao Li, Yao Mu, Jiangmiao Pang, Yu Qiao, et al. Internvla-m1: A spatially guided vision-language-action framework for generalist robot policy. *arXiv preprint arXiv:2510.13778*, 2025.

[12] Open X-Embodiment Collaboration, Abby O'Neill, Abdul Rehman, Abhinav Gupta, Abhiram Maddukuri, Abhishek Gupta, Abhishek Padalkar, Abraham Lee, Acorn Pooley, Agrim Gupta, Ajay Mandlekar, Ajinkya Jain, Albert Tung, Alex Bewley, Alex Herzog, Alex Irpan, Alexander Khazatsky, Anant Rai, Anchit Gupta, Andrew Wang, Andrey Kolobov, Anikait Singh, Animesh Garg, Aniruddha Kembhavi, Annie Xie, Anthony Brohan, Antonin Raffin, Archit Sharma, Arefeh Yavary, Arhan Jain, Ashwin Balakrishna, Ayzaan Wahid, Ben Burgess-Limerick, Beomjoon Kim, Bernhard Schlkopf, Blake Wulfe, Brian Ichter, Cewu Lu, Charles Xu, Charlotte Le, Chelsea Finn, Chen Wang, Chenfeng Xu, Cheng Chi, Chenguang Huang, Christine Chan, Christopher Agia, Chuer Pan, Chuyuan Fu, Coline Devin, Danfei Xu, Daniel Morton, Danny Driess, Daphne Chen, Deepak Pathak, Dhruv Shah, Dieter Bhler, Dinesh Jayaraman, Dmitry Kalashnikov, Dorsa Sadigh, Edward Johns, Ethan Foster, Fangchen Liu, Federico Ceola, Fei Xia, Feiyu Zhao, Felipe Vieira Frujeri, Freek Stulp, Gaoyue Zhou, Gaurav S. Sukhatme, Gautam Salhotra, Ge Yan, Gilbert Feng, Giulio Schiavi, Glen Berseth, Gregory Kahn, Guangwen Yang, Guanzhi Wang, Hao Su, Hao-Shu Fang, Haochen Shi, Henghui Bao, Heni Ben Amor, Henrik I Christensen, Hiroki Furuta, Homanga Bharadhwaj, Homer Walke, Hongjie Fang, Huy Ha, Igor Mordatch, Ilija Radosavovic, Isabel Leal, Jacky Liang, Jad Abou-Chakra, Jaehyung Kim, Jaimyn Drake, Jan Peters, Jan Schneider, Jasmine Hsu, Jay Vakil, Jeannette Bohg, Jeffrey Bingham, Jeffrey Wu, Jensen Gao, Jiaheng Hu, Jiajun Wu, Jialin Wu, Jiankai Sun, Jianlan Luo, Jiayuan Gu, Jie Tan, Jihoon Oh, Jimmy Wu, Jingpei Lu, Jingyun Yang, Jitendra Malik, Joo Silvrio, Joey Hejna, Jonathan Booher, Jonathan Tompson, Jonathan Yang, Jordi Salvador, Joseph J. Lim, Junhyek Han, Kaiyuan Wang, Kanishka Rao, Karl Pertsch, Karol Hausman, Keegan Go, Keerthana Gopalakrishnan, Ken Goldberg, Kendra Byrne, Kenneth Oslund, Kento Kawaharazuka, Kevin Black, Kevin Lin, Kevin Zhang, Kiana Ehsani, Kiran Lekkala, Kirsty Ellis, Krishan Rana, Krishnan Srinivasan, Kuan Fang, Kunal Pratap Singh, Kuo-Hao Zeng, Kyle Hatch, Kyle Hsu, Laurent Itti, Lawrence Yunliang Chen, Lerrel Pinto, Li Fei-Fei, Liam Tan, Linxi "Jim" Fan, Lionel Ott, Lisa Lee, Luca Weihs, Magnum Chen, Marion Lepert, Marius Memmel, Masayoshi Tomizuka, Masha Itkina, Mateo Guaman Castro, Max Spero, Maximilian Du, Michael Ahn, Michael C. Yip, Mingtong Zhang, Mingyu Ding, Minho Heo, Mohan Kumar Srirama, Mohit Sharma, Moo Jin Kim, Muhammad Zubair Irshad, Naoaki Kanazawa, Nicklas Hansen, Nicolas Heess, Nikhil J Joshi, Niko Suenderhauf, Ning Liu, Norman Di Palo, Nur Muhammad Mahi Shafiullah, Oier Mees, Oliver Kroemer, Osbert Bastani, Pannag R Sanketi, Patrick "Tree" Miller, Patrick Yin, Paul Wohlhart, Peng Xu, Peter David Fagan, Peter Mitrano, Pierre Sermanet, Pieter Abbeel, Priya Sundaesan, Qiuyu Chen, Quan Vuong, Rafael Rafailov, Ran Tian, Ria Doshi, Roberto Mart'in-Mart'in, Rohan Baijal, Rosario Scalise, Rose Hendrix, Roy Lin, Runjia Qian, Ruohan Zhang, Russell Mendonca, Rutav Shah, Ryan Hoque, Ryan Julian, Samuel Bustamante, Sean Kirmani, Sergey Levine, Shan Lin, Sherry Moore, Shikhar Bahl, Shivin Dass, Shubham Sonawani, Shubham Tulsiani, Shuran Song, Sichun Xu, Siddhant Haldar, Siddharth Karamcheti, Simeon Adegbola, Simon Guist, Soroush Nasiriany, Stefan Schaal, Stefan Welker, Stephen Tian, Subramanian Ramamoorthy, Sudeep Dasari, Suneel Belkhale, Sungjae Park, Suraj Nair, Suvir Mirchandani, Takayuki Osa, Tanmay Gupta, Tatsuya Harada, Tatsuya Matsushima, Ted Xiao, Thomas Kollar, Tianhe Yu, Tianli Ding, Todor Davchev, Tony Z. Zhao, Travis Armstrong, Trevor Darrell, Trinity Chung, Vidhi Jain, Vikash Kumar, Vincent Vanhoucke, Vitor Guizilini, Wei Zhan, Wenxuan Zhou, Wolfram Burgard, Xi Chen, Xiangyu Chen, Xiaolong Wang, Xinghao Zhu, Xinyang Geng, Xiyuan Liu, Xu Liangwei, Xuanlin Li, Yansong Pang, Yao Lu, Yecheng Jason Ma, Yejin Kim,

Yevgen Chebotar, Yifan Zhou, Yifeng Zhu, Yilin Wu, Ying Xu, Yixuan Wang, Yonatan Bisk, Yongqiang Dou, Yoonyoung Cho, Youngwoon Lee, Yuchen Cui, Yue Cao, Yueh-Hua Wu, Yujin Tang, Yuke Zhu, Yunchu Zhang, Yunfan Jiang, Yunshuang Li, Yunzhu Li, Yusuke Iwasa, Yutaka Matsuo, Zehan Ma, Zhuo Xu, Zichen Jeff Cui, Zichen Zhang, Zipeng Fu, and Zipeng Lin. Open X-Embodiment: Robotic learning datasets and RT-X models. <https://arxiv.org/abs/2310.08864>, 2023.

[13] Dima Damen, Hazel Doughty, Giovanni Maria Farinella, Sanja Fidler, Antonino Furnari, Evangelos Kazakos, Davide Moltisanti, Jonathan Munro, Toby Perrett, Will Price, et al. The epic-kitchens dataset: Collection, challenges and baselines. *IEEE Transactions on Pattern Analysis and Machine Intelligence*, 43(11):4125–4141, 2020.

[14] Shengliang Deng, Mi Yan, Songlin Wei, Haixin Ma, Yuxin Yang, Jiayi Chen, Zhiqi Zhang, Taoyu Yang, Xuheng Zhang, Wenhao Zhang, et al. Graspvla: a grasping foundation model pre-trained on billion-scale synthetic action data. *arXiv preprint arXiv:2505.03233*, 2025.

[15] Zicong Fan, Omid Taheri, Dimitrios Tzionas, Muhammed Kocabas, Manuel Kaufmann, Michael J. Black, and Otmar Hilliges. ARCTIC: A dataset for dexterous bimanual hand-object manipulation. In *Proceedings IEEE Conference on Computer Vision and Pattern Recognition (CVPR)*, 2023.

[16] Hao-Shu Fang, Hongjie Fang, Zhenyu Tang, Jirong Liu, Chenxi Wang, Junbo Wang, Haoyi Zhu, and Cewu Lu. Rh20t: A comprehensive robotic dataset for learning diverse skills in one-shot, 2023. URL <https://arxiv.org/abs/2307.00595>.

[17] Raghav Goyal, Samira Ebrahimi Kahou, Vincent Michalski, Joanna Materzynska, Susanne Westphal, Heuna Kim, Valentin Haenel, Ingo Fruend, Peter Yianilos, Moritz Mueller-Freitag, et al. The “something something” video database for learning and evaluating visual common sense. In *Proceedings of the IEEE international conference on computer vision*, pages 5842–5850, 2017.

[18] Kristen Grauman, Andrew Westbury, Eugene Byrne, Zachary Chavis, Antonino Furnari, Rohit Girdhar, Jackson Hamburger, Hao Jiang, Miao Liu, Xingyu Liu, et al. Ego4d: Around the world in 3,000 hours of egocentric video. In *Proceedings of the IEEE/CVF conference on computer vision and pattern recognition*, pages 18995–19012, 2022.

[19] Kristen Grauman, Andrew Westbury, Lorenzo Torresani, Kris Kitani, Jitendra Malik, Triantafyllos Afouras, Kumar Ashutosh, Vijay Baiyya, Siddhant Bansal, Bikram Boote, et al. Ego-exo4d: Understanding skilled human activity from first-and third-person perspectives. In *Proceedings of the IEEE/CVF Conference on Computer Vision and Pattern Recognition*, pages 19383–19400, 2024.

[20] Jonathan Ho, Ajay Jain, and Pieter Abbeel. Denoising diffusion probabilistic models. *arXiv preprint arxiv:2006.11239*, 2020.

[21] Ryan Hoque, Peide Huang, David J Yoon, Mouli Sivapurapu, and Jian Zhang. Egodex: Learning dexterous manipulation from large-scale egocentric video. *arXiv preprint arXiv:2505.11709*, 2025.

[22] Yuhang Huang, Jiazhao Zhang, Shilong Zou, XInwang Liu, Ruizhen Hu, and Kai Xu. Ladi-wm: A latent diffusion-based world model for predictive manipulation. *arXiv preprint arXiv:2505.11528*, 2025.

[23] Physical Intelligence, Kevin Black, Noah Brown, James Darpinian, Karan Dhabalia, Danny Driess, Adnan Esmail, Michael Equi, Chelsea Finn, Niccolò Fusai, et al.  $\pi_{0.5}$ : a vision-language-action model with open-world generalization. *arXiv preprint arXiv:2504.16054*, 2025.

[24] Yuming Jiang, Siteng Huang, Shengke Xue, Yaxi Zhao, Jun Cen, Sicong Leng, Kehan Li, Jiayan Guo, Kexiang Wang, Mingxiu Chen, et al. Rynnvla-001: Using human demonstrations to improve robot manipulation. *arXiv preprint arXiv:2509.15212*, 2025.

[25] Siddharth Karamcheti, Suraj Nair, Annie S Chen, Thomas Kollar, Chelsea Finn, Dorsa Sadigh, and Percy Liang. Language-driven representation learning for robotics. In *Robotics: Science and Systems (RSS)*, 2023.

[26] Alexander Khazatsky, Karl Pertsch, Suraj Nair, Ashwin Balakrishna, Sudeep Dasari, Siddharth Karamcheti, Soroush Nasiriany, Mohan Kumar Srirama, Lawrence Yunliang Chen, Kirsty Ellis, et al. Droid: A large-scale in-the-wild robot manipulation dataset. *Robotics: Science and Systems (RSS)*, 2024.

[27] Moo Jin Kim, Karl Pertsch, Siddharth Karamcheti, Ted Xiao, Ashwin Balakrishna, Suraj Nair, Rafael Rafailov, Ethan P Foster, Pannag R Sanketi, Quan Vuong, et al. Openvla: An open-source vision-language-action model. In *Conference on Robot Learning*, pages 2679–2713. PMLR, 2025.

[28] LejuRobotics. Let:full-size humanoid robot real-world dataset. [https://huggingface.co/datasets/LejuRobotics/let\\_dataset](https://huggingface.co/datasets/LejuRobotics/let_dataset), 2025.

[29] Chengshu Li, Ruohan Zhang, Josiah Wong, Cem Gokmen, Sanjana Srivastava, Roberto Martn-Martn, Chen Wang, Gabrael Levine, Wensi Ai, Benjamin Martinez, Hang Yin, Michael Lingelbach, Minjune Hwang, Ayano Hiranaka, Sujay Garlanka, Arman Aydin, Sharon Lee, Jiankai Sun, Mona Anvari, Manasi Sharma, Dhruva Bansal, Samuel Hunter, Kyu-Young Kim, Alan Lou, Caleb R Matthews, Ivan Villa-Renteria, Jerry Huayang Tang, Claire Tang, Fei Xia, Yunzhu Li, Silvio Savarese, Hyowon Gweon, C. Karen Liu, Jiajun Wu, and Li Fei-Fei. Behavior-1k: A human-centered, embodied ai benchmark with 1,000 everyday activities and realistic simulation. *arXiv preprint arXiv:2403.09227*, 2024.

[30] Shuang Li, Yihuai Gao, Dorsa Sadigh, and Shuran Song. Unified video action model. *arXiv preprint arXiv:2503.00200*, 2025.

[31] Yue Liao, Pengfei Zhou, Siyuan Huang, Donglin Yang, Shengcong Chen, Yuxin Jiang, Yue Hu, Jingbin Cai,

Si Liu, Jianlan Luo, et al. Genie envisioner: A unified world foundation platform for robotic manipulation. *arXiv preprint arXiv:2508.05635*, 2025.

[32] Songming Liu, Lingxuan Wu, Bangguo Li, Hengkai Tan, Huayu Chen, Zhengyi Wang, Ke Xu, Hang Su, and Jun Zhu. Rdt-1b: a diffusion foundation model for bimanual manipulation. *arXiv preprint arXiv:2410.07864*, 2024.

[33] Yun Liu, Haolin Yang, Xu Si, Ling Liu, Zipeng Li, Yuxiang Zhang, Yebin Liu, and Li Yi. Taco: Benchmarking generalizable bimanual tool-action-object understanding. In *Proceedings of the IEEE/CVF Conference on Computer Vision and Pattern Recognition*, pages 21740–21751, 2024.

[34] Yunze Liu, Yun Liu, Che Jiang, Kangbo Lyu, Weikang Wan, Hao Shen, Boqiang Liang, Zhoujie Fu, He Wang, and Li Yi. Hoi4d: A 4d egocentric dataset for category-level human-object interaction. In *Proceedings of the IEEE/CVF Conference on Computer Vision and Pattern Recognition*, pages 21013–21022, 2022.

[35] Hao Luo, Yicheng Feng, Wanpeng Zhang, Sipeng Zheng, Ye Wang, Haoqi Yuan, Jiazheng Liu, Chaoyi Xu, Qin Jin, and Zongqing Lu. Being-h0: vision-language-action pre-training from large-scale human videos. *arXiv preprint arXiv:2507.15597*, 2025.

[36] Jiangran Lyu, Ziming Li, Xuesong Shi, Chaoyi Xu, Yizhou Wang, and He Wang. Dywa: Dynamics-adaptive world action model for generalizable non-prehensile manipulation. *arXiv preprint arXiv:2503.16806*, 2025.

[37] Yecheng Jason Ma, Shagun Sodhani, Dinesh Jayaraman, Osbert Bastani, Vikash Kumar, and Amy Zhang. Vip: Towards universal visual reward and representation via value-implicit pre-training. *arXiv preprint arXiv:2210.00030*, 2022.

[38] Suraj Nair, Aravind Rajeswaran, Vikash Kumar, Chelsea Finn, and Abhinav Gupta. R3m: A universal visual representation for robot manipulation. In *Conference on Robot Learning (CoRL)*. PMLR, 2022.

[39] Soroush Nasiriany, Abhiram Maddukuri, Lance Zhang, Adeet Parikh, Aaron Lo, Abhishek Joshi, Ajay Mandlekar, and Yuke Zhu. Robocasa: Large-scale simulation of everyday tasks for generalist robots. In *Robotics: Science and Systems*, 2024.

[40] NVIDIA, Johan Bjorck, Nikita Cherniadev, Fernando Castaeda, Xingye Da, Runyu Ding, Linxi "Jim" Fan, Yu Fang, Dieter Fox, Fengyuan Hu, Spencer Huang, Joel Jang, Zhenyu Jiang, Jan Kautz, Kaushil Kundalia, Lawrence Lao, Zhiqi Li, Zongyu Lin, Kevin Lin, Guilin Liu, Edith Llontop, Loic Magne, Ajay Mandlekar, Avnish Narayan, Soroush Nasiriany, Scott Reed, You Liang Tan, Guanzhi Wang, Zu Wang, Jing Wang, Qi Wang, Jiannan Xiang, Yuqi Xie, Yinzen Xu, Zhenjia Xu, Seonghyeon Ye, Zhiding Yu, Ao Zhang, Hao Zhang, Yizhou Zhao, Ruijie Zheng, and Yuke Zhu. GR00T N1: An open foundation model for generalist humanoid robots. In *ArXiv Preprint*, March 2025.

[41] Octo Model Team, Dibya Ghosh, Homer Walke, Karl Pertsch, Kevin Black, Oier Mees, Sudeep Dasari, Joey Hejna, Charles Xu, Jianlan Luo, Tobias Kreiman, You Liang Tan, Lawrence Yunliang Chen, Pannag Sanketi, Quan Vuong, Ted Xiao, Dorsa Sadigh, Chelsea Finn, and Sergey Levine. Octo: An open-source generalist robot policy. In *Proceedings of Robotics: Science and Systems*, Delft, Netherlands, 2024.

[42] Abhishek Padalkar, Acorn Pooley, Ajinkya Jain, Alex Bewley, Alex Herzog, Alexander Irpan, Alexander Khazatsky, Anant Rai, Anikait Singh, Anthony Brohan, et al. Open x-embodiment: Robotic learning datasets and RT-X models. *arXiv preprint arXiv:2310.08864*, 2023.

[43] William Peebles and Saining Xie. Scalable diffusion models with transformers. *arXiv preprint arXiv:2212.09748*, 2022.

[44] Heqian Qiu, Zhaofeng Shi, Lanxiao Wang, Huiyu Xiong, Xiang Li, and Hongliang Li. Egome: Follow me via egocentric view in real world. *arXiv e-prints*, pages arXiv–2501, 2025.

[45] Javier Romero, Dimitrios Tzionas, and Michael J. Black. Embodied hands: Modeling and capturing hands and bodies together. *ACM Transactions on Graphics, (Proc. SIGGRAPH Asia)*, 36(6), November 2017.

[46] Oriane Siméoni, Huy V. Vo, Maximilian Seitzer, Federico Baldassarre, Maxime Oquab, Cijo Jose, Vasil Khalidov, Marc Szafraniec, Seungeun Yi, Michaël Ramamondjisoa, Francisco Massa, Daniel Haziza, Luca Wehrstedt, Jianyuan Wang, Timothée Darcret, Théo Moutakanni, Leonel Santana, Claire Roberts, Andrea Vedaldi, Jamie Tolan, John Brandt, Camille Couprie, Julien Mairal, Hervé Jégou, Patrick Labatut, and Piotr Bojanowski. DINOv3, 2025. URL <https://arxiv.org/abs/2508.10104>.

[47] starVLA Contributors. Starvla: A lego-like codebase for vision-language-action model developing. GitHub repository, 1 2025. URL <https://github.com/starVLA/starVLA>.

[48] Galaxea Team. Galaxea g0: Open-world dataset and dual-system vla model. *arXiv preprint arXiv:2509.00576v1*, 2025.

[49] Xin Wang, Taein Kwon, Mahdi Rad, Bowen Pan, Ishani Chakraborty, Sean Andrist, Dan Bohus, Ashley Feniello, Bugra Tekin, Felipe Vieira Frujeri, et al. Holoassist: an egocentric human interaction dataset for interactive ai assistants in the real world. In *Proceedings of the IEEE/CVF International Conference on Computer Vision*, pages 20270–20281, 2023.

[50] Kun Wu, Chengkai Hou, Jiaming Liu, Zhengping Che, Xiaozhu Ju, Zhiqin Yang, Meng Li, Yinuo Zhao, Zhiyuan Xu, Guang Yang, et al. Robomind: Benchmark on multi-embodiment intelligence normative data for robot manipulation. In *Robotics: Science and Systems (RSS) 2025*. Robotics: Science and Systems Foundation, 2025. URL <https://www.roboticsproceedings.org/rss21/p152.pdf>.

[51] Shihan Wu, Xuecheng Liu, Shaoxuan Xie, Pengwei Wang, Xinghang Li, Bowen Yang, Zhe Li, Kai Zhu, Hongyu Wu, Yiheng Liu, et al. Robocon: An open-

sourced bimanual robotic data collection for integrated manipulation. *arXiv preprint arXiv:2511.17441*, 2025.

[52] An Yang, Anfeng Li, Baosong Yang, Beichen Zhang, Binyuan Hui, Bo Zheng, Bowen Yu, Chang Gao, Chengan Huang, Chenxu Lv, Chujie Zheng, Dayiheng Liu, Fan Zhou, Fei Huang, Feng Hu, Hao Ge, Haoran Wei, Huan Lin, Jialong Tang, Jian Yang, Jianhong Tu, Jianwei Zhang, Jianxin Yang, Jiaxi Yang, Jing Zhou, Jingren Zhou, Junyang Lin, Kai Dang, Keqin Bao, Kexin Yang, Le Yu, Lianghao Deng, Mei Li, Mingfeng Xue, Mingze Li, Pei Zhang, Peng Wang, Qin Zhu, Rui Men, Ruize Gao, Shixuan Liu, Shuang Luo, Tianhao Li, Tianyi Tang, Wenbiao Yin, Xingzhang Ren, Xinyu Wang, Xinyu Zhang, Xuancheng Ren, Yang Fan, Yang Su, Yichang Zhang, Yinger Zhang, Yu Wan, Yuqiong Liu, Zekun Wang, Zeyu Cui, Zhenru Zhang, Zhipeng Zhou, and Zihan Qiu. Qwen3 technical report. *arXiv preprint arXiv:2505.09388*, 2025.

[53] Ruihan Yang, Qinxi Yu, Yecheng Wu, Rui Yan, Borui Li, An-Chieh Cheng, Xueyan Zou, Yunhao Fang, Xuxin Cheng, Ri-Zhao Qiu, et al. Egovla: Learning vision-language-action models from egocentric human videos. *arXiv preprint arXiv:2507.12440*, 2025.

[54] Xinyu Zhan, Lixin Yang, Yifei Zhao, Kangrui Mao, Hanlin Xu, Zenan Lin, Kailin Li, and Cewu Lu. Oakink2: A dataset of bimanual hands-object manipulation in complex task completion. In *Proceedings of the IEEE/CVF Conference on Computer Vision and Pattern Recognition*, pages 445–456, 2024.

[55] Hongxiang Zhao, Xingchen Liu, Mutian Xu, Yiming Hao, Weikai Chen, and Xiaoguang Han. Taste-rob: Advancing video generation of task-oriented hand-object interaction for generalizable robotic manipulation. In *Proceedings of the Computer Vision and Pattern Recognition Conference*, pages 27683–27693, 2025.

[56] Tony Z Zhao, Vikash Kumar, Sergey Levine, and Chelsea Finn. Learning fine-grained bimanual manipulation with low-cost hardware. In *Robotics: Science and Systems (RSS)*, 2023.

[57] Zhenyu Zhao, Hongyi Jing, Xiawei Liu, Jiageng Mao, Abha Jha, Hanwen Yang, Rong Xue, Sergey Zakharov, Vitor Guizilini, and Yue Wang. Humanoid everyday: A comprehensive robotic dataset for open-world humanoid manipulation, 2025. URL <https://arxiv.org/abs/2510.08807>.

[58] Ruijie Zheng, Jing Wang, Scott Reed, Johan Bjorck, Yu Fang, Fengyuan Hu, Joel Jang, Kaushil Kundalia, Zongyu Lin, Loic Magne, et al. Flare: Robot learning with implicit world modeling. *arXiv preprint arXiv:2505.15659*, 2025.

[59] Gaoyue Zhou, Hengkai Pan, Yann LeCun, and Lerrel Pinto. Dino-wm: World models on pre-trained visual features enable zero-shot planning. *arXiv preprint arXiv:2411.04983*, 2024.

[60] Chuning Zhu, Raymond Yu, Siyuan Feng, Benjamin Burchfiel, Paarth Shah, and Abhishek Gupta. Unified world models: Coupling video and action diffusion for pretraining on large robotic datasets. *arXiv preprint arXiv:2504.02792*, 2025.

## APPENDIX A DETAILS OF MODEL

We employ Qwen3-VL-4B-Instruct [52] as the joint language and vision encoder to extract high-level semantic representations. Visual observations are encoded using DINOv3-ViT-s [46]. During pretraining, we freeze both the VLM and the DINOv3 image encoder to leverage the strong priors from the pretrained language and vision models while allowing the MM-DiT to be trained thoroughly on the downstream structure. In the subsequent finetuning stage, we unfreeze the VLM to enable end-to-end adaptation and further improve overall performance.

Additionally, the MM-DiT is conditioned on a short history of two timesteps, comprising both past DINO-encoded observations and actions, to effectively capture temporal dynamics. Table V presents the detailed configurations of the model and the hyperparameters used during training.

Parameter	Value
<b>Model</b>	
VLM	Qwen3-VL [52]
Observation Encoder	DINOv3-ViT-s [46]
Hidden Size	1536
Layers	16
Attention Heads	32
Image Shape	(224, 224, 3)
Latent Image Shape	(14, 14, 384)
Action Chunk	16
<b>Training</b>	
Batch Size	32 * 48 (pretraining) 12 * 8 (finetuning)
Learning Rate	$1e^{-4}$
Optimizer	AdamW
Weight Decay	$1e^{-5}$
Betas	[0.9, 0.95]
Epsilon	$1e^{-8}$
LR Schedule	cosine w/ min lr
Min LR	$5e^{-7}$

TABLE V: Model and Training configuration hyperparameters

## APPENDIX B

### DETAILED RESULTS ON THE SIMULATION BENCHMARK

#### A. Evaluation Setup and Model Description.

All methods are evaluated on the full set of 24 RoboCasaGR1 [39] tasks, with 51 evaluation trials per task. Unless otherwise specified, models are finetuned using 1,000 demonstrations per task and optimized under the same training paradigm to isolate architectural differences.

We summarize the evaluated models below:

- **UWM**: A 140M-parameter Unified World Model [60], serving as a lightweight baseline.
- **UWM-XL**: A 1B-parameter UWM variant equipped with Qwen3-VL [52] for joint language-vision encoding.
- **UWM+MM-DiT**: UWM-L with its DiT backbone replaced by our MM-DiT architecture.
- **GR00T-N1.6** [40]: The original GR00T policy model without explicit dynamics modeling.

- **StarVLA**: A GR00T variant following StarVLA [47], replacing the original VLM with Qwen3-VL and trained from scratch on RoboCasa.
- **GR00T-EI10k**: A strong reproduced baseline pretrained on our EI-10k high-quality subset with Qwen3-VL, where VLM parameters are unfrozen during finetuning.
- **LDA (DiT)**: An ablated version of LDA replacing MM-DiT with a standard DiT backbone.
- **LDA-1B**: The full Latent Dynamics Action model with MM-DiT, designed to model action-induced state transitions in a structured latent space.

#### B. Task-Level Results and Analysis.

Table VI reports detailed per-task success rates. LDA consistently outperforms GR00T across contact-rich and cluttered rearrangement tasks, with particularly large gains in scenarios requiring precise placement and closing actions, such as PnP Bottle To Cabinet Close (76 % vs. 51.5%), PnP Can To Drawer Close (71% vs. 13%), and PnP Milk To Microwave Close (52% vs. 14%).

As illustrated in Fig. 12, GR00T frequently fails due to a lack of anticipation of post-action consequences. For example, after placing an object inside a container, GR00T often retracts its arm along a trajectory that collides with the object, causing it to tip over. In contrast, LDA anticipates such interactions and generates trajectories that preserve object stability throughout the entire manipulation sequence.

The largest improvements are observed in novel-object rearrangement tasks involving transfers across surfaces and containers (e.g., *Cuttingboard*  $\rightarrow$  *Basket/Cardboardbox*, *Placemat*  $\rightarrow$  *Plate/Tieredshelf*, and *Tray*  $\rightarrow$  *Cardboardbox/Plate/Pot*). These tasks require adaptive contact handling and trajectory correction under clutter, where LDA shows clear advantages. While GR00T remains competitive on a small subset of simple pick-and-place tasks with minimal environmental interaction, these cases are limited. Overall, LDAs higher average success rate (55.4 % vs. 47.6 %) reflects a systematic advantage in complex and contact-rich manipulation scenarios rather than isolated gains.

## APPENDIX C DETAILS REGARDING REAL-WORLD EXPERIMENT

#### A. Real-world Setup.

We conduct real-world experiments on two humanoid platforms: the Galbot G1 and the Unitree G1, as shown in Fig.13. The Galbot G1, with two 7-DoF arms, is equipped with two interchangeable end-effectors: two-finger parallel-jaw grippers and 22-DoF SharpaWave dexterous hands. The Unitree G1 uses 10-DoF BrainCo hands. In all real-robot configurations, the policy receives visual input only from an egocentric head-mounted camera, providing a first-person view of the workspace.

#### B. Task description and evaluation protocol.

To validate the effectiveness of our method on physical systems, we evaluate eight representative manipulation tasks

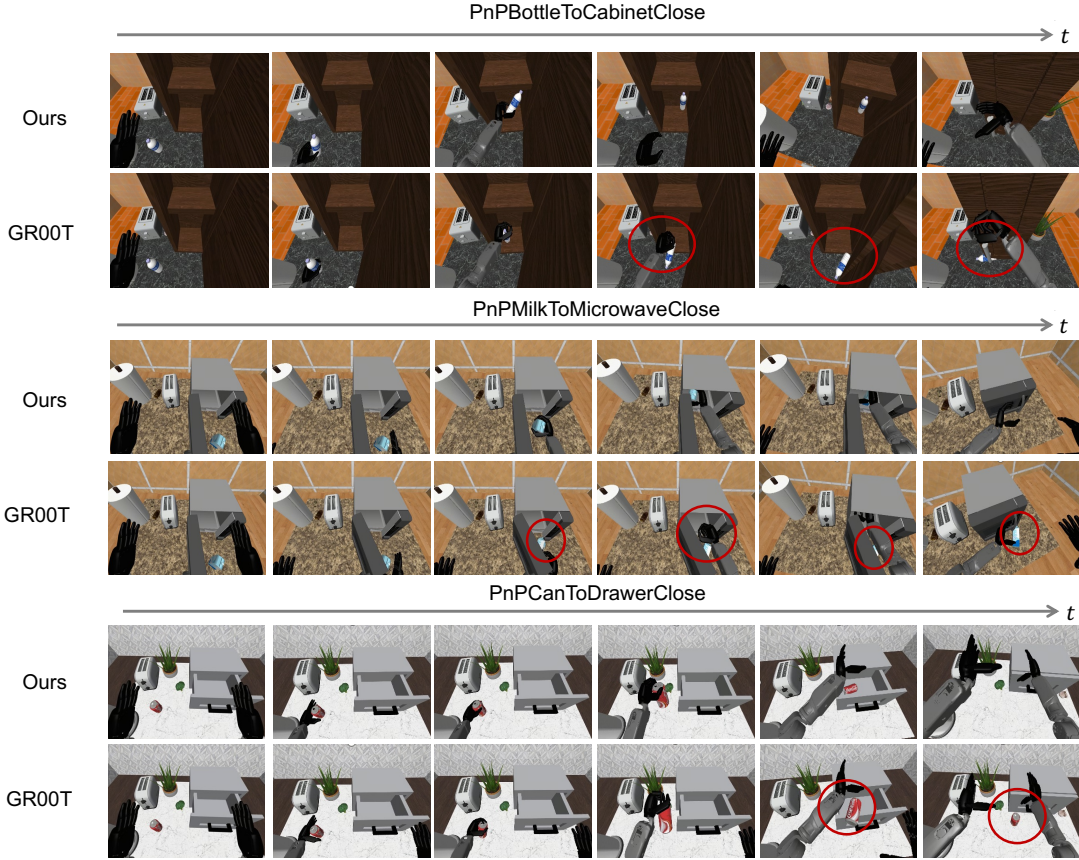


Fig. 12: Qualitative comparison between our model and GR00T [40] on RoboCasa-GR1 [39] manipulation tasks. Three representative tasks demonstrate our model’s superior robustness in object grasping and placement accuracy. Critical failure modes of GR00T, including grasp slippage, misaligned object placement, and collision during manipulation, are highlighted with circles, while our model consistently achieves successful task completion.

involving single-arm, dual-arm coordination, tool use, and contact-rich interactions. For object generalization, movable objects are randomized within predefined spatial regions while several supporting objects (e.g., baskets, dustpans, and trash bins) remain fixed to isolate task-specific manipulation challenges rather than compounding errors from initial grasp failures. All experiments are conducted in-domain, and each trial is terminated after 200 seconds if unsuccessful. Task success is defined using task-specific criteria such as successful object placement, execution of full procedural steps, or normalized scoring metrics for partial completion in long-horizon tasks. We evaluate each task over independent trials. The corresponding training data volume and success criteria for each task are summarized in Table VII.

### C. More Analysis.

To validate the efficacy of our proposed approach, we conducted a comprehensive comparison against two baseline policies: GR00T-N1.6 [40] and  $\pi_{0.5}$  [23]. Our method (LDA) demonstrates superior performance across all four evaluated categories: Pick & Place, Contact-rich Manipulation, Fine Manipulation, and Long-horizon Manipulation.

**Performance on Basic Grasping Tasks.** In standard Pick & Place scenarios, LDA achieves a dominant success rate, reaching 90.0% on the “handover” task, significantly outperforming  $\pi_{0.5}$  [23] (70.0%) and nearly doubling the success rate of GR00T-N1.6 [40] (50.0%). This indicates that our policy has learned a more robust grasping primitive and achieve better few-shot adaptation on unseen Galbot robot, benefiting from larger-scale cross-embodiment learning.

**Robustness in Contact-Rich and Fine Manipulation.** The advantages of LDA become increasingly pronounced in tasks requiring precise dynamic interaction. In Contact-rich Manipulation, such as “flip the box,” LDA achieves a 60.0% success rate compared to just 20.0% for GR00T-N1.6 [40]. This suggests that LDA effectively models the complex contact dynamics required to manipulate objects without slippage or instability, whereas the baselines likely struggle with the discontinuous nature of the contact forces. Similarly, in Fine Manipulation tasks like “pouring,” which demand continuous closed-loop feedback, our method sustains an 80.0% success rate, surpassing the best baseline ( $\pi_{0.5}$  [23]) by 20 percentage points.

model	UWM	UWM-XL	UWM+MMDiT	GR00T	StarVLA	GR00T-EI10k	LDA(DiT)	LDA
PnP Bottle To Cabinet Close	27	41	49	51.5	46	<b>69</b>	<b>65</b>	<b>76</b>
PnP Can To Drawer Close	22	53	55	13	<b>80</b>	<b>61</b>	59	<b>71</b>
PnP Cup To Drawer Close	18	12	43	8.5	<b>54</b>	<b>47</b>	40	41
PnP Milk To Microwave Close	22	25	33	14	<b>48</b>	<b>75</b>	47	<b>52</b>
PnP Potato To Microwave Close	16	29	18	<b>41.5</b>	28	<b>41</b>	39	<b>41</b>
PnP Wine To Cabinet Close	31	24	25	16.5	46	<b>51</b>	49	<b>57</b>
PnP Novel From Cuttingboard To Basket	8	18	10	<b>58</b>	48	43	55	<b>65</b>
PnP Novel From Cuttingboard To Cardboardbox	8	14	16	46.5	40	39	<b>57</b>	<b>69</b>
PnP Novel From Cuttingboard To Pan	24	20	27	<b>68.5</b>	<b>68</b>	67	65	<b>75</b>
PnP Novel From Cuttingboard To Pot	16	25	20	<b>65</b>	52	53	<b>57</b>	<b>61</b>
PnP Novel From Cuttingboard To Tieredbasket	10	10	6	46.5	<b>56</b>	29	39	<b>51</b>
PnP Novel From Placemat To Basket	8	16	14	<b>58.5</b>	42	45	37	<b>53</b>
PnP Novel From Placemat To Bowl	12	10	14	<b>57.5</b>	44	<b>55</b>	53	<b>55</b>
PnP Novel From Placemat To Plate	10	12	10	<b>63</b>	48	<b>57</b>	51	<b>59</b>
PnP Novel From Placemat To Tieredshelf	2	2	2	<b>28.5</b>	18	<b>20</b>	22	<b>24</b>
PnP Novel From Plate To Bowl	12	8	14	<b>57</b>	<b>60</b>	49	<b>57</b>	53
PnP Novel From Plate To Cardboardbox	2	10	8	43.5	<b>50</b>	<b>61</b>	43	43
PnP Novel From Plate To Pan	10	20	16	51	<b>54</b>	51	49	<b>55</b>
PnP Novel From Plate To Plate	22	27	25	<b>78.7</b>	<b>70</b>	67	59	61
PnP Novel From Tray To Cardboardbox	20	25	20	<b>51.5</b>	38	49	<b>59</b>	<b>65</b>
PnP Novel From Tray To Plate	12	18	16	<b>71</b>	56	57	<b>57</b>	<b>63</b>
PnP Novel From Tray To Pot	18	25	20	<b>64.5</b>	50	<b>63</b>	53	55
PnP Novel From Tray To Tieredbasket	6	16	16	<b>57</b>	36	<b>55</b>	39	51
PnP Novel From Tray To Tieredshelf	4	2	4	<b>31.5</b>	16	<b>31</b>	22	<b>33</b>
Average	14.3	19.3	20.0	47.6	47.8	<b>51.3</b>	48.9	<b>55.4</b>

TABLE VI: Results on RoboCasa-GR1 [39] benchmark. UWM-S: UWM [60] with 100M parameters. UWM-L: UWM with 1B parameters, using Qwen3-VL [52] as the joint encoder for language instructions and visual inputs. UWM-MMDiT: UWM-L with its DiT [43] backbone replaced by our MM-DiT architecture. QwenGR00T: GR00T [40] equipped with Qwen3-VL as its System 2 module. GR00T\*: GR00T [40] pretrained on our dataset and equipped with Qwen3-VL as its System 2 module. LDA (DiT): Our LDA model with the MM-DiT replaced by a standard DiT. During finetuning on RoboCasa, the VLM is unfrozen to enable end-to-end adaptation.

**Capabilities in Long-Horizon Planning.** The most striking distinction emerges in the Long-horizon Manipulation category. While baseline methods achieve moderate success on the relatively simple sweep the table task, they completely fail on the more complex throw rubbish task, registering a 0.0% success rate. In stark contrast, LDA achieves a 35.0% success rate, demonstrating robustness in multi-stage, temporally extended scenarios. This performance gap reveals a fundamental limitation of existing approaches: their inability to manage compounding errors over long action sequences due to a lack of explicit dynamics modeling. LDA’s success stems from its capacity to reason about the physical consequences of actions across time, maintain temporal consistency in latent states, and recover from intermediate deviationscapabilities that are essential for real-world, multi-step manipulation. Crucially, this advantage is rooted in LDAs dynamics-aware architecture, which aligns predicted visual features with underlying physical transitions and mitigates covariate shift through structured temporal modeling. Collectively, these results validate that explicitly modeling latent dynamics is not merely beneficial but *necessary* for reliable, generalizable robotic manipulation in complex, real-world settings.

**Capabilities in Dexterous Manipulation.** LDA consistently outperforms baselines on both low-DoF and high-DoF hands, with the performance gap becoming more pronounced as task difficulty and dexterity requirements increase. For low-

DoF hands, LDA already demonstrates strong robustness on tasks involving tool use and force-sensitive interactions. On *Pick Bottle*, LDA achieves a 90% success rate, substantially higher than  $\pi_{0.5}$  (20%) and GR00T-N1.6 (75%). On *Pull Nail*, which requires precise force direction and stable contact maintenance, LDA reaches 80% success, while  $\pi_{0.5}$  completely fails and GR00T-N1.6 achieves only 40%. Notably, all methods perform well on *Open Macbook*, suggesting that tasks with strong geometric affordances and limited contact ambiguity are less challenging even for baseline policies. The advantage of LDA becomes even more evident with high-DoF hands, where action spaces are larger and control errors accumulate more easily. On *Pick Bread*, LDA attains a 70% success rate, outperforming GR00T-N1.6 (20%) and  $\pi_{0.5}$  (10%). The gap further widens on *Flip Bread*, a highly dexterous task requiring coordinated finger motion and continuous contact reasoning, where LDA achieves 90% success while both baselines remain at only 10%. These results highlight LDAs superior ability for high-dimensional control and contact-rich dexterous manipulation. Unlike baseline methods that rely primarily on reactive policies, LDA benefits from dynamics-aware latent representations that capture fine-grained physical interactions over time. This enables more stable control, improved contact reasoning, and effective recovery from transient failurescapabilities that are critical for dexterous manipulation with complex, multi-DoF robotic hands.

Task Abbreviation	Description	Test Protocol
Pick Vegetable	Pick a plastic pepper and place it into a basket using the left gripper. Pepper is randomized within a $15 \times 30$ cm region.	10 trials; success if placed in basket
Handover	Left gripper grasps a bottle and passes it to the right gripper, which places it into a basket. Bottle randomized within $15 \times 30$ cm.	10 trials; success if placed in basket
Wipe Board	Use an eraser to remove marker writing from a whiteboard. Writing area randomized within $25 \times 40$ cm.	10 trials; scored from 0–5 based on cleaning completeness
Flip Box	Flip an upside-down storage box to upright using bimanual manipulation. Box randomized within $2 \times 4$ cm.	10 trials; success if fully flipped
Water Flower (pouring)	grasp a watering bottle and pour water into a flower pot. Pot randomized within $15 \times 15$ cm.	10 trials; success if pouring posture is achieved with spout above pot
Knock the block with hammer (pnp2)	grasp a hammer with a very thin handle and then knock the specific block. Hammer randomized within $15 \times 15$ cm.	60 trials; only if both the grasp and knock succeed.
Sweep Table	Sweep ten nails into a dustpan using a broom and dustpan. Nail positions randomized within $10 \times 25$ cm.	10 trials; success rate is computed as the proportion of nails collected in the dustpan.
Throw Rubbish	Pick paper balls, place them into a dustpan, and dump them into a trash can. Paper balls are randomized within a $20 \times 25$ cm area.	10 trials; success rate is computed as the proportion of paper balls successfully dumped into the trash can.

TABLE VII: Real-world gripper manipulation for Galbot task configurations. All tasks are evaluated in-domain with a timeout of 200 seconds per trial.

Task Abbreviation	Description	Test Protocol
Pick Bottle	Pick up a plastic bottle and place it onto a fixed target region using the right hand. Bottle position is randomized.	20 trials; success if bottle is upright and its base overlaps at least half of the target region
Open MacBook	Left hand stabilizes the base while the right hand opens the hinge by pushing the upper edge. Initial opening angle is randomized.	20 trials; success if opening angle exceeds 75% of maximum
Pull Nail	Use a claw hammer held by the right hand to extract a nail from the surface. Hammer pose is randomized.	10 trials; scored with partial credit: 0.25 for locating, 0.5 for single-claw removal, 1.0 for full claw removal
Pick Bread	Pick a bread item and place it into a plate using the right hand. Three bread types are used with equal distribution.	10 trials; success if bread is placed into the plate
Flip Bread	Flip a long bread using a spatula held by the right hand. Bread pose is randomized over a large region.	10 trials; 1.0 if flipped on first attempt, 0.5 if second, 0 otherwise

TABLE VIII: Dexterous hand manipulation tasks and evaluation protocols.

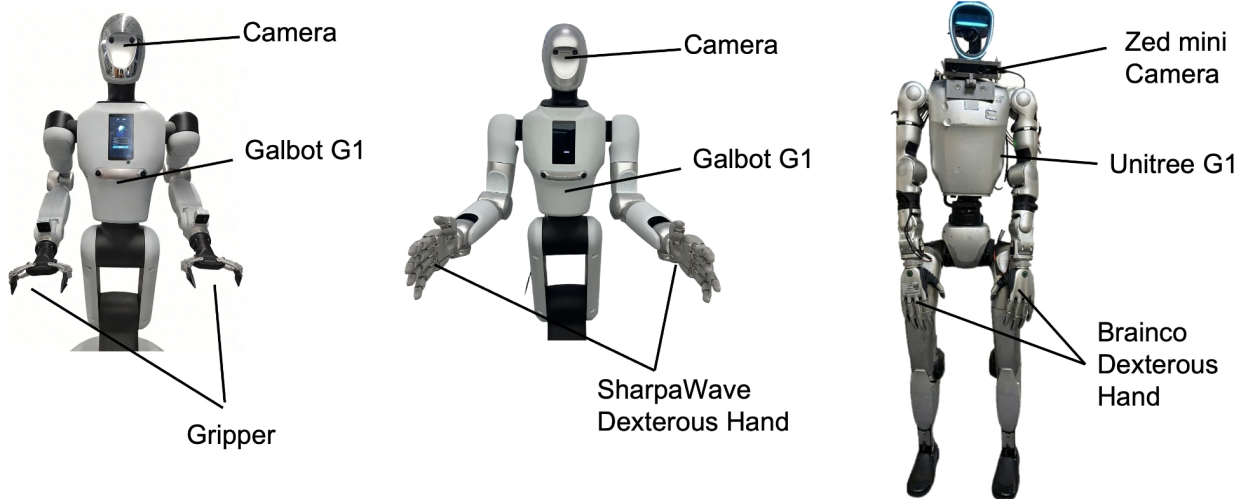


Fig. 13: Real-world robot platforms used in our physical experiments. From left to right: (1) Galbot G1 equipped with a standard two-finger parallel gripper for basic grasping tasks; (2) Galbot G1 fitted with the SharpaWave dexterous hand (22 DoF) for fine manipulation; (3) Unitree G1 mounted with the BrainCo dexterous hand (10 DoF) and a Zed Mini camera. This multi-platform setup demonstrates the generalization capability of our LDA model across diverse robot morphologies and end-effectors.

#### APPENDIX D DETAILS OF EI-30K.

##### A. Data Processing Pipeline for Robot and Human Datasets

To ensure consistency and usability across heterogeneous robot and human datasets, we design a standardized data processing pipeline that converts raw recordings into a unified representation suitable for effective learning of both policy and dynamics. The pipeline consists of three main stages: dataset standardization, coordinate alignment and cleaning, and post-processing for training.

*a) Dataset Standardization:* All raw datasets are first converted into the common LeRobot [8] 2.1 format. This format includes:

- **End-effector poses:** 6D position and orientation for both hands (human) or manipulators (robot);
- **Hand articulation:** 21-point MANO keypoints for human hands (when available) and binary or continuous gripper states for robots;
- **Camera parameters:** intrinsic and extrinsic matrices enabling reprojection across coordinate frames;
- **Task and temporal metadata:** task identifiers, episode boundaries and timestamps.

During this stage, all sequences are uniformly resampled to 10 Hz, and structured metadata files are generated to preserve the alignment between frames and their semantic annotations, ensuring temporal coherence and task-aware data organization for downstream training.

After standardization of LeRobot format, we implement an easy-to-use Dataset class for the following data process pipeline to harmonize heterogeneous action data across diverse datasets.

```
def __init__(self, dataset: str, eef_in_world: int, has_mano: bool):
    self.dataset = dataset
    self.eef_in_world = eef_in_world
    # 1 if wrist in world coordinates
    self.has_mano = has_mano
    self.eef_offset = {hand: np.eye(4) for hand in HAND_KEYS}
    self.eef_keys = HAND_KEYS

def get_wrist(self, df: pd.DataFrame) -> dict[str, np.ndarray]:
    pass

def get_mano_or_gripper(self, df: pd.DataFrame):
    pass
```

*b) Coordinate Alignment and Data Cleaning:* Human and robot datasets often employ inconsistent coordinate frame definitions. To unify them, particularly the end-effector (EEF) representations, we apply the following alignment and cleaning steps:

- **End-effector coordinate alignment:** For each dataset, we define a canonical EEF frame (e.g., at the wrist or gripper center). All recorded hand or manipulator poses are transformed into this common frame using a dataset-specific rigid offset, estimated through geometric inspection or visual validation.
- **Camera motion decoupling:** For sequences captured in a moving camera frame, hand trajectories are reprojected into a fixed world coordinate system to eliminate artifacts caused by camera motion.
- **Keypoint standardization:** Human hand poses without native MANO keypoints are converted into the standard 21-point MANO representation, expressed relative to the aligned wrist frame.
- **Data validation:** Hand visibility is verified using an off-

```
class EmbodiedDataset:
```

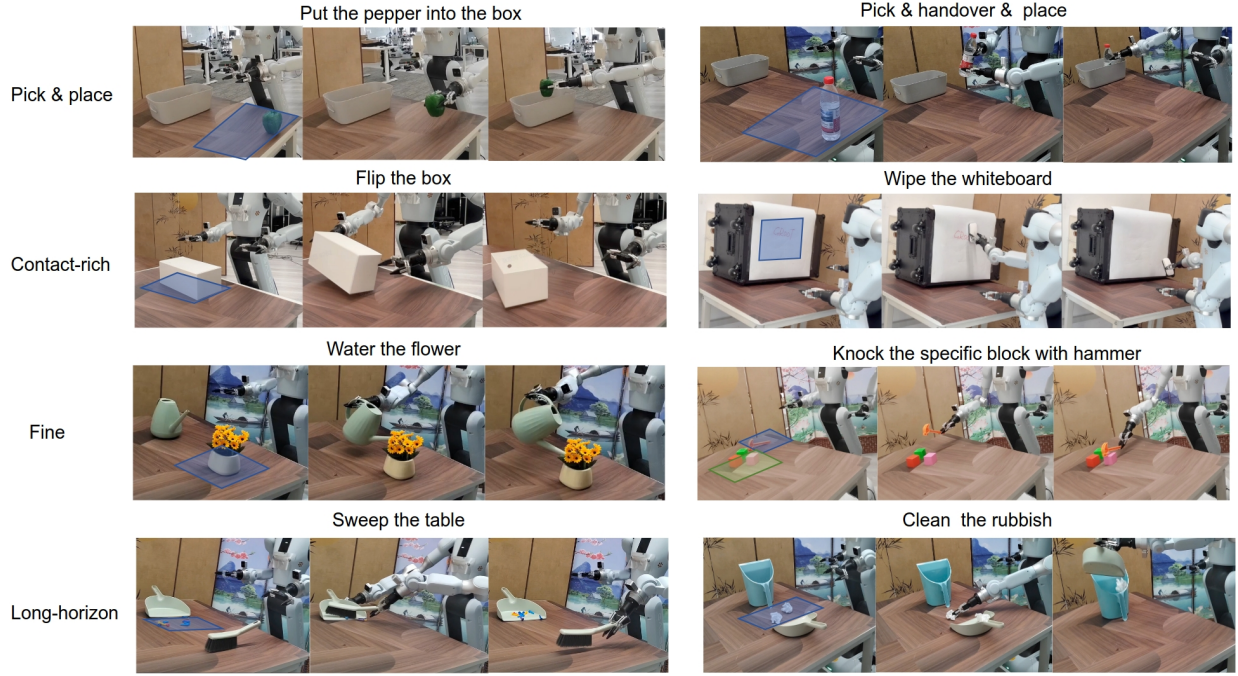


Fig. 14: Task descriptions for the Galbot G1 robot equipped with a standard two-finger parallel-jaw gripper, spanning four manipulation categories.

the-shelf detector; frames with occluded, truncated, or kinematically invalid hand data are discarded to ensure annotation reliability.

For robot datasets, we further normalize actuation signals: gripper widths are scaled to a consistent range (e.g., [0, 1]), and joint encodings are harmonized to match a unified kinematic convention.

*c) Data Cleaning:* Textual annotations are unified into a structured format that explicitly describes the environmental context, per-hand actions (left/right), and high-level task objectives. When original annotations are inconsistent or missing, we leverage vision-language models to generate coherent, semantically aligned instructions. Finally, all processed datasets are organized by agent type (human or robot) and accompanied by comprehensive metadata files detailing task definitions, episode boundaries, and dataset statistics. This standardized pipeline ensures a consistent, interoperable data representation across domains enabling robust, scalable training of dexterous manipulation policies that generalize across embodiment and task complexity.

#### B. Data Composition.

Our training data spans four complementary categories, totaling more than 30,000 hours of egocentric experience:

*a) Real-world Robot Data :* This category includes large-scale physical robot execution logs. We primarily leverage *Open X-Embodiment* [12] and *Agibot World* [6] for general-purpose manipulation. To enhance hardware-specific capabilities, we incorporate *Humanoid Everyday* [57] for bipedal locomotion dynamics and *Galaxea* [48] for high-fidelity dexterous tasks. Additionally, we include *RoboCOIN* [51] despite its

Data Type	Source / Sub-dataset	Duration (h)
<b>Real-world Robot</b>	Open X-Embodiment [12]	3000
	Agibot World [6]	3276
	RoboMIND [50]	305
	Humanoid Everyday [57]	30
	RoboCOIN [51]	500
	Galaxea [48]	500
<b>Simulated Robot</b>	LET [28]	1000
	InternData-A1 [11]	7433
<b>Ego Human (w/ Action)</b>	Behavior-1k [29]	1200
	Ego4D [18]	3670
	Epic-Kitchens [13]	100
	Ego-Exo4d [19]	1286
	SSV2 [17]	240
	EgoDex [21]	830
	HOT3D [2]	16
	HoloAssist [49]	166
	OAKINK2 [54]	6.5
	TACO [33]	3.2
<b>Ego Human (Actionless)</b>	HOI4D [34]	7.6
	ARCTIC [15]	2.3
	Egocentric-10k [1]	10000
	RH20T-human [16]	100
<b>Total</b>		<b>30k+</b>

TABLE IX: Composition of the Embodied Interaction Dataset (EI-30K). The dataset is categorized into four main types, aggregating over 30k hours of data.

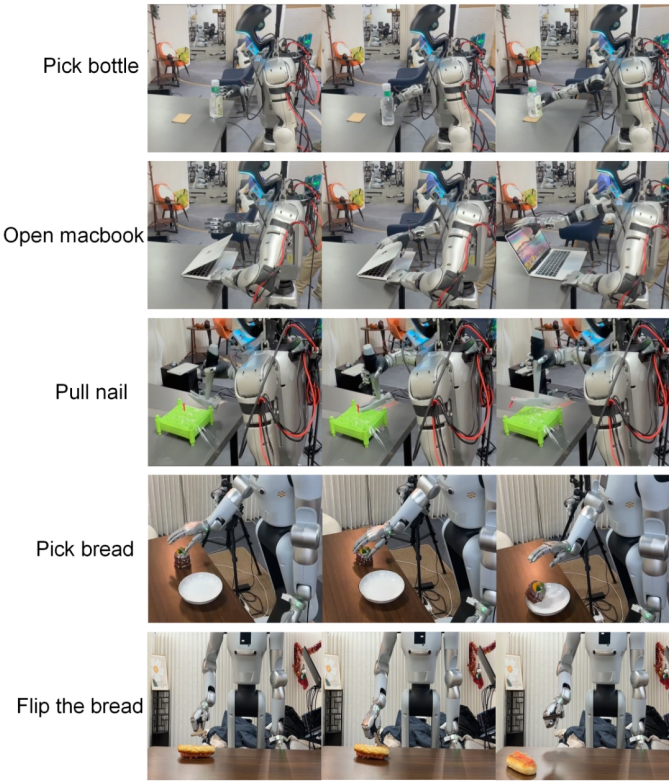


Fig. 15: Dexterous manipulation task description across two robotic platforms. Top three rows: Unitree robot equipped with BrainCo hands performing bottle placement, MacBook opening, and nail extraction. Bottom two rows: Galbot robot utilizing SharpaWave hands executing bread placement and flipping tasks.

noisier action labels, as it provides valuable diverse environment explorations.

*b) Simulated Robot Data:* To provide dense, noise-free supervision, we use high-quality simulated trajectories. The majority comes from *InternData-A1* [11], which offers large-scale automated generation of locomotion and basic manipulation sequences. *Behavior-1k* [29] further contributes long-horizon task demonstrations in simulated household environments, enabling the model to learn complex task hierarchies.

*c) Egocentric Human Data with Actions:* This subset bridges human intent and robot-executable actions. We draw from large-scale datasets such as *Ego4D* [18], *Epic-Kitchens* [13], *Ego-Exo4d* [19] and *SSV2* [17] focusing on object-interaction segments. High-precision sources like *EgoDex* [21] and *HOT3D* [2] provide fine-grained 3D hand poses and contact information, critical for learning extrinsic dexterity.

*d) Egocentric Human Data without Actions:* Representing the largest source of visual diversity, this category consists of first-person observations. *Egocentric-10k* [1] serves as the primary source, covering a broad spectrum of daily activities. Additional datasets like *RH20T-human* [16] and *Taste-Rob* [55] contribute domain-specific visual priors. Although

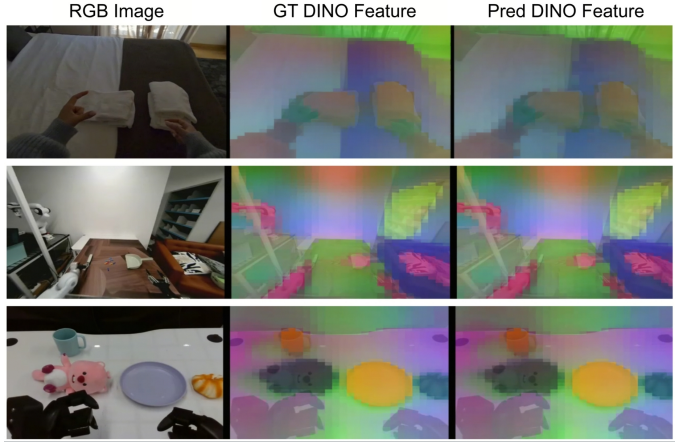


Fig. 16: DINO Feature Prediction Visualization. Left column: Original RGB input images. Middle column: Ground-truth DINO features extracted by DINOv3 [46]. Right column: DINO features predicted by our model.

these trajectories lack explicit action labels, they provide a powerful self-supervised signal for learning world dynamics, visual affordances, and temporal structure.

## APPENDIX E DETAILS OF OTHER EXPERIMENTS

### A. Action-Conditioned Attention Visualization.

We provide additional details on how action-conditioned attention maps are computed and interpreted. Our visualization is based on the Diffusion Transformer (DiT) [43] backbone, where visual tokens and action embeddings interact through shared self-attention layers.

For a given observation, we extract attention maps from the middle transformer blocks, where high-level semantic and geometric information is most prominent. Conditioned on an active action primitive (e.g., “Push Right”), we compute the attention weights  $A_1$ , which quantify the influence of each spatial token on the predicted latent transition. To establish a reference, we generate a baseline attention map  $A_2$  by replacing the action embedding with a *No-Op* (static) command.

We then compute the absolute difference:

$$\Delta A = |A_1 - A_2|,$$

which isolates attention changes induced purely by the action condition. This subtraction effectively removes generic visual saliency (e.g., high-contrast edges or background objects) and highlights regions whose relevance emerges only when a specific action is applied.

As illustrated in Fig. 11, the resulting difference maps consistently emphasize contact regions, force application points, and anticipated motion trajectories. For example, in the “Push Right” task, attention shifts toward the gripper-object contact interface and the direction of expected displacement. This behavior demonstrates that the DiT dynamically re-weights visual tokens based on the physics implied by the action, rather than passively encoding static appearance.

### *B. Visualization of Latent Forward Dynamics*

We provide additional qualitative visualizations to illustrate the forward dynamics learned by LDA. These qualitative results complement the quantitative analysis and provide further evidence that LDA learns structured, dynamics-aware latent representations suitable for long-horizon reasoning and control.